


RESEARCH ARTICLE

In vivo structural connectome of arousal and motor brainstem nuclei by 7 Tesla and 3 Tesla MRI

María Guadalupe García-Gomar^{1,2}  | Kavita Singh¹ | Simone Cauzzo^{1,3} | Marta Bianciardi^{1,4}

¹Brainstem Imaging Laboratory, Department of Radiology, Athinoula A. Martinos Center for Biomedical Imaging, Massachusetts General Hospital and Harvard Medical School, Boston, Massachusetts, USA

²Escuela Nacional de Estudios Superiores, Juriquilla, Universidad Nacional Autónoma de México, Querétaro, Mexico

³Life Sciences Institute, Sant'Anna School of Advanced Studies, Pisa, Italy

⁴Division of Sleep Medicine, Harvard University, Boston, Massachusetts, USA

Correspondence

María Guadalupe García-Gomar, Department of Radiology, Athinoula A. Martinos Center for Biomedical Imaging, Massachusetts General Hospital and Harvard Medical School, Building 149, Room 2132, 13th Street, Charlestown, MA 02129, USA.
Email: mgarciagomar@mgh.harvard.edu

Marta Bianciardi, Department of Radiology, Athinoula A. Martinos Center for Biomedical Imaging, Massachusetts General Hospital and Harvard Medical School, Building 149, Room 2301, 13th Street, Charlestown, MA 02129, USA.
Email: martab@mgh.harvard.edu

Funding information

Harvard-Mind-Brain-Behavior-Faculty-Award; MGH-Clafin-Distinguished-Scholar; National Institute of Biomedical Imaging and Bioengineering, Grant/Award Number: K01EB019474; National Institute on Aging, Grant/Award Number: R01AG063982;

Abstract

Brainstem nuclei are key participants in the generation and maintenance of arousal, which is a basic function that modulates wakefulness/sleep, autonomic responses, affect, attention, and consciousness. Their mechanism is based on diffuse pathways ascending from the brainstem to the thalamus, hypothalamus, basal forebrain and cortex. Several arousal brainstem nuclei also participate in motor functions that allow humans to respond and interact with the surrounding through a multipathway motor network. Yet, little is known about the structural connectivity of arousal and motor brainstem nuclei in living humans. This is due to the lack of appropriate tools able to accurately visualize brainstem nuclei in conventional imaging. Using a recently developed in vivo probabilistic brainstem nuclei atlas and 7 Tesla diffusion-weighted images (DWI), we built the structural connectome of 18 arousal and motor brainstem nuclei in living humans ($n = 19$). Furthermore, to investigate the translatability of our findings to standard clinical MRI, we acquired 3 Tesla DWI on the same subjects, and measured the association of the connectome across scanners. For both arousal and motor circuits, our results showed high connectivity within brainstem nuclei, and with expected subcortical and cortical structures based on animal studies. The association between 3 Tesla and 7 Tesla connectivity values was good, especially within the brainstem. The resulting structural connectome might be used as a baseline to better understand arousal and motor functions in health and disease in humans.

KEYWORDS

7 Tesla MRI, arousal network, brainstem, human structural connectome, motor network

Abbreviations of brainstem nuclei used as seeds and additional brainstem nuclei used as targets: CLI-RLI, caudal-rostral linear raphe; CnF, cuneiform; DR, dorsal raphe; ION, inferior olivary nucleus; isRt, isthmic reticular formation; LC, locus coeruleus; LDTg-CGPn, laterodorsal tegmental nucleus-central gray of the rhombencephalon; MnR, median raphe nucleus; mRt, mesencephalic reticular formation; PAG, periaqueductal gray; PMnR, paramedian raphe nucleus; PnO-PnC, pontine reticular nucleus oral part-pontine reticular nucleus caudal part; PTg, pedunculotegmental nucleus; RN1, red nucleus-subregion1; RN2, red nucleus-subregion2; SN1, substantia nigra-subregion1; SN2, substantia nigra-subregion2; SubC, subcoeruleus nucleus; IC, inferior colliculus; iMRT, inferior medullary reticular formation; LPB, lateral parabrachial nucleus; MiTg-PBG, microcellular tegmental nucleus-prabigeminal nucleus; MPB, medial parabrachial nucleus; PCRtA, parvocellular reticular nucleus alpha part; RMg, raphe magnus; ROB, raphe obscurus; RPa, raphe pallidus; SC, superior colliculus; sMRT, superior medullary reticular formation; SOC, superior olivary complex; Ve, vestibular nuclei complex; VSM, viscerosensory motor nuclei complex; VTA-PBP, ventral tegmental area-parabrachial pigmented nucleus.

This is an open access article under the terms of the [Creative Commons Attribution-NonCommercial-NoDerivs](https://creativecommons.org/licenses/by-nc-nd/4.0/) License, which permits use and distribution in any medium, provided the original work is properly cited, the use is non-commercial and no modifications or adaptations are made.

© 2022 The Authors. *Human Brain Mapping* published by Wiley Periodicals LLC.

National Institute on Deafness and Other
Communication Disorders, Grant/Award
Number: R21DC015888

1 | INTRODUCTION

In the past 70 years several brainstem nuclei have been implicated in the generation and maintenance of arousal based on animal stimulation/lesions studies (Moruzzi & Magoun, 1949; Satpute et al., 2019) and on their ability to modulate the cortex either through direct connectivity pathways to the cortex or through the thalamus (reticular and intralaminar nuclei), hypothalamus and basal forebrain

(Olszewski & Baxter, 2014; Parvizi, 2001; Satpute et al., 2019). A diagram showing the expected structural afferent and efferent connections of arousal brainstem nuclei is shown in Figure 1; note that both widespread connections and local interconnectivity are present.

In seminal studies (Moruzzi & Magoun, 1949), the mesopontine reticular formation in the brainstem has been first recognized as the central node of the ascending arousal system, able to induce and maintain wakeful arousal in animals. Nowadays, we know that the

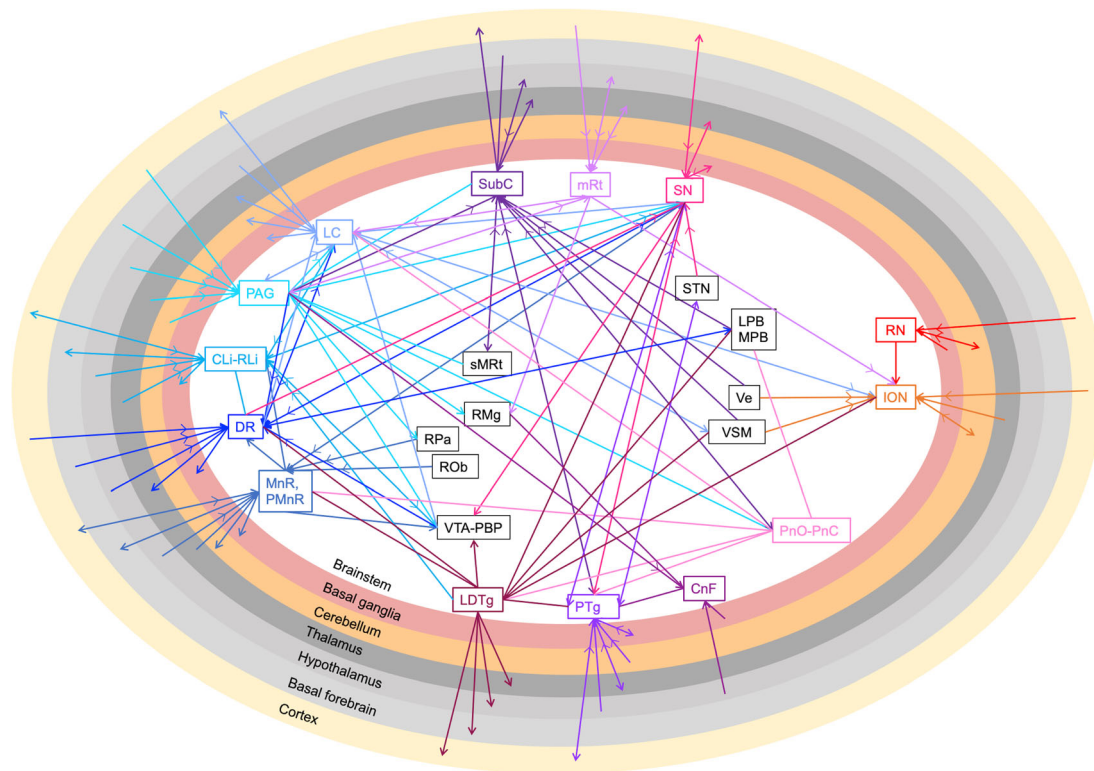


FIGURE 1 Structural connectivity of arousal and motor brainstem nuclei based on literature. Brainstem nuclei are displayed within the white central oval, specifically with brainstem seeds in its outer part and brainstem targets (black) in its inner part. Arousal seed brainstem nuclei are shown on the left (cool colors), motor seed brainstem nuclei are shown on the right (warm colors), and nuclei involved in both functions are shown in the middle (pink and purple colors). Afferents and efferents (Olszewski & Baxter, 2014) are indicated with arrows; lack of directionality information in the literature is shown with line segments without arrows. Arousal brainstem nuclei (Olszewski & Baxter, 2014) show widespread structural connectivity with the cortex, basal forebrain, hypothalamus, and thalamus, as well as high interconnectivity. Motor brainstem nuclei show connectivity with the cortex, cerebellum, basal ganglia, and other brainstem nuclei also involved in motor function. List of abbreviations of 18 arousal and motor brainstem nuclei used as seeds: CLi-RLi, caudal–rostral linear raphe; CnF, cuneiform nucleus; DR, dorsal raphe; ION, inferior olivary nucleus; isRt, isthmic reticular formation; LC, locus coeruleus; LDTg-CGPn, laterodorsal tegmental nucleus–central gray of the rhombencephalon; MnR, median raphe nucleus; mRt, mesencephalic reticular formation; PAG, periaqueductal gray; PMnR, paramedian raphe nucleus; PnO-PnC, pontine reticular nucleus, oral part–pontine reticular nucleus caudal part; PTg, pedunculotegmental nucleus; RN1, red nucleus-subregion1; RN2, red nucleus-subregion2; SN1, substantia nigra-subregion1; SN2, substantia nigra-subregion2; SubC, subcoeruleus nucleus. List of abbreviations of 15 additional autonomic/limbic/pain and sensory brainstem nuclei used only as targets: IC, inferior colliculus; iMRt, inferior medullary reticular formation; LPB, lateral parabrachial nucleus; MiTg-PBG, microcellular tegmental nucleus–prabigeminal nucleus; MPB, medial parabrachial nucleus; PCRTA, parvocellular reticular nucleus alpha part; RMg, raphe magnus; ROb, raphe obscurus; RPa, raphe pallidus; SC, superior colliculus; sMRt, superior medullary reticular formation; SOC, superior olivary complex; Ve, vestibular nuclei complex; VSM, viscerosensory motor nuclei complex; VTA-PBP, ventral tegmental area–parabrachial pigmented nucleus. List of abbreviations as in the Introduction; additional abbreviation: STN, subthalamic nucleus (diencephalic nucleus).

mesopontine reticular formation comprises several nuclei, such as the pontine reticular formation nuclei (oral and caudal part, PnO-PnC), the mesencephalic reticular formation (mRt), cuneiform nucleus (CnF), and isthmus reticular formation (isRt) (Olszewski & Baxter, 2014).

Later studies rather identified nuclei neighboring the reticular formation as key players in the generation and maintenance of arousal. Interestingly, these nuclei are also involved in a wide variety of phenomena including sleep, autonomic function, affect and attention (Olszewski & Baxter, 2014; Satpute et al., 2019). These include raphe nuclei, that is, the dorsal raphe (DR), the median raphe, (MnR), the paramedian raphe (PMnR) and the caudal-rostral linear nucleus of the raphe (CLi-RLi) (Olszewski & Baxter, 2014), known to promote wakefulness by activating the cerebral cortex via serotonergic receptors. They also play a role in stress, conflict, anxiety, initiation, and promotion of fight-or-flight responses (Edlow et al., 2012). Moreover, an arousal function has been recognized to cholinergic tegmental nuclei (Olszewski & Baxter, 2014; Parvizi, 2001; Saper et al., 2001), such as the laterodorsal tegmental nucleus (LDTg), also implicated in limbic function, and the pedunculotegmental nucleus (PTg), also influencing the sleep-wake cycle (García-Rill et al., 2019). Further, in the dorsal brainstem, LC and PAG are part of a network of wake-promoting pathways also controlling breathing, as they collect projections from C1 neurons in the ventrolateral medulla to trigger chemosensation-induced arousal (Guyenet & Abbott, 2013). LC is also involved in motivation and attention (Satpute et al., 2019), and PAG in pain, limbic functions and in the switch between rapid eye movement (REM) and non-REM sleep (Benarroch, 2012; Lu, 2006). Finally, the subcoeruleus (SubC) (Boeve et al., 2007; Olszewski & Baxter, 2014) and substantia nigra (with its subregions 1 and 2, SN1, SN2) (Bianciardi et al., 2021; Boeve et al., 2007) also participate in arousal and sleep.

Interestingly, several arousal nuclei are also involved in motor function, which is necessary for the interaction with the environment and for the expression of behavior. Specifically, the CnF and the PTg form the mesencephalic locomotor region. The PTg has been involved in the control of posture and gait, and recently also in reflex reactions (García-Rill et al., 2019); and the CnF in the generation of locomotion by activating central pattern generators in the spinal cord (Takakusaki et al., 2003). The PnO-PnC and the mRt are involved in eye (e.g., gaze) and head movements (Graf & Ugolini, 2006). The SubC generates the REM sleep atonia (Boeve et al., 2007). Invasive tracers in rodents have suggested that LDTg is involved in oculomotor mechanisms (Cornwall et al., 1990). The substantia nigra, located in the midbrain, plays an integral role in the generation of voluntary motor actions (Olszewski & Baxter, 2014). Interestingly, arousal and motor brainstem nuclei, such as CnF, PTg PnO-PnC, mRt, SubC, SN, and LDTg, are expected to connect (see diagram in Figure 1) to arousal regions (Olszewski & Baxter, 2014; Parvizi, 2001; Satpute et al., 2019), as well as to motor (Merel et al., 2019; Olszewski & Baxter, 2014) regions, such as the basal ganglia, cerebellum, motor, and premotor cortex.

In spite of their crucial function in arousal and motor control and of their involvement in disorder of consciousness, sleep disorders, and movement disorders, little is known in living humans about their

anatomical interconnectivity, and their connectivity with other cortical and subcortical structures (Cacciola, Bertino, et al., 2019; Cacciola, Milardi, et al., 2019; Delano-Wood et al., 2015; Edlow et al., 2012; Tang et al., 2018). This is because of the difficulty in localizing these deep and small regions of the brain in MRI of living humans, owing to limited sensitivity and spatial resolution of conventional diffusion weighted imaging.

To this end, current work aimed to develop a structural connectome of arousal and motor nuclei by the use of a recently developed probabilistic atlas of the above mentioned arousal and motor brainstem nuclei in living humans (Bianciardi et al., 2015, 2018; García-Gomar et al., 2021; Singh et al., 2021), as well as of high resolution (1.7 mm isotropic) diffusion weighted MRI at 7 Tesla acquired on healthy subjects. To provide a more comprehensive view of the motor circuit, we included the above mentioned motor nuclei, as well as nuclei involved in the olivo-rubro cerebellar motor pathways. These are the inferior olivary nucleus (ION), and the red nucleus (RN, with its two subregions RN1 and RN2), which are interconnected, project to the cerebellum, and are involved in integrating sensory-motor information to provide feedback to cerebellar neurons (Olszewski & Baxter, 2014). We performed probabilistic tractography using arousal and motor brainstem nuclei as seeds (stated above), and cortical and sub-cortical regions encompassing the whole grey matter as targets. We also used as targets brainstem nuclei involved in other functions such as autonomic/limbic/nociceptive and sensory (Bianciardi et al., 2016, 2018; García-Gomar et al., 2019; García-Gomar et al., 2021). Further, to verify the translatability of the structural connectome approach to clinical settings, we also acquired on the same subjects diffusion weighted MRI at 3 Tesla with conventional spatial resolution (2.5 mm isotropic), and compared the connectomes across scanners.

Finally, as a validation of the obtained structural connectome, we built a diagram of arousal nuclei and a diagram of motor nuclei, by defining the circuit nodes based on system neuroscience literature, and verified the presence of expected connectivity based on animal and human studies.

2 | METHODS

2.1 | Study participants and overview

Twenty healthy subjects (10 males and 10 females, age 29.5 ± 1.1 years) underwent MRI under the Massachusetts General Hospital Institutional Review Board approval. All the subjects provided written informed consent in accordance with the declaration of Helsinki. Each subject performed two MRI sessions, one at 7 Tesla (Magnetom, Siemens Healthineers, Erlangen, Germany) and one at 3 Tesla (Connectom, Siemens Healthineers, Erlangen, Germany). The order of the session was randomized across subjects. Notably, for the purposes of this study, at 3 Tesla we did not exploit the advanced 3 Tesla Connectom scanner capabilities for diffusion imaging; rather, we used a conventional diffusion MRI sequence. During both MRI sessions, the

subjects' head motion was minimized using foam pads placed near the ears and under the head. One subject was excluded due to poor image quality (low sensitivity in the center of the brain and higher field inhomogeneities in the brainstem, which resulted in small glyph amplitudes of the fiber orientation distribution function, as shown in Figure S1).

2.2 | 7 Tesla data acquisition

All images were acquired with a custom-built 32-channel receive and volume-transmit coil (Keil et al., 2010) providing enhanced sensitivity in the brainstem as compared with commercial coils. For each participant *diffusion-weighted imaging (DWI)* was acquired using a common single-shot 2D spin-echo echo-planar-imaging (EPI, using a prototype sequence which supports unipolar diffusion-encoding) approach with an isotropic resolution of 1.7 mm, 82 contiguous slices that provided full brain coverage, echo time of 66.8 ms, repetition time of 7.4 s, phase-encoding along an anterior/posterior direction, bandwidth of 1456 Hz/pixel, partial-Fourier of 6/8, 60 diffusion-directions, b -value of 2500 s/mm², seven interspersed “ b_0 ” images (T_2 -weighted, non-diffusion-weighted, b -value of 0 s/mm²) and an acquisition-time of 8'53". To perform distortion-correction we also acquired seven “ b_0 ” images with opposite (i.e., posterior/anterior) phase-encoding direction.

2.3 | 3 Tesla data acquisition

A custom-built 64-channel receive coil and volume transmit coil was used (Keil et al., 2013). These data, acquired on the same subjects as at 7 Tesla, were used to verify the clinical translatability of our tractography based connectomes. Specifically, we acquired conventional DWIs with an isotropic resolution of 2.5 mm, 64 contiguous slices that provided full brain coverage, echo time of 84 ms, repetition time of 7300 ms, phase encoding along an anterior/posterior direction, bandwidth of 2422 Hz/pixel, partial Fourier of 7/8, 60 diffusion-directions, b -value of 2500 s/mm² and an acquisition time of 9'29". To perform distortion-correction, we also acquired eight “ b_0 ” images with opposite phase-encoding direction. Additionally, to perform cortical and subcortical regions parcellation, a T_1 -weighted multi-echo-MPRAGE image (MEMPRAGE) was acquired with an isotropic resolution of 1 mm, echo time of [1.69, 3.5, 5.3, 7.2] ms, repetition time of 2.53 s, inversion time of 1.5 s, flip angle of 7°, FOV of 256 × 256 × 176 mm³, bandwidth of 650 Hz/pixel, GeneRalized Autocalibrating Partial Parallel Acquisition (GRAPPA) factor of 3, sagittal slice orientation, phase encoding along an anterior–posterior direction and an acquisition time of 4'28".

2.4 | 7 Tesla data preprocessing

DWIs were de-noised (Manjón et al., 2013), motion and distortion-corrected (FSL, topup/eddy). Tensor invariants (such as fractional

anisotropy, FA, and non-diffusion T_2 -weighted S_0 signal, S_0) were computed using FSL (fsl.fmrib.ox.ac.uk/fsl/fslwiki/).

2.5 | 3 Tesla MEMPRAGE processing

The root-mean-square of the MEMPRAGE image across echo times was computed, it was rotated to standard-orientation (“RPI”), and bias field corrected using SPM8 (fil.ion.ucl.ac.uk/spm/software/spm8/). Then, using FSL, we extracted the brain and cropped the most inferior slices containing the spinal-cord (in order to aid its coregistration to native DWI-space by the use of an affine boundary-based transformation, as explained below).

2.6 | Definition of seed regions for tractography computation

We used as *seed regions* the probabilistic atlas labels of 18 brainstem nuclei involved in arousal and motor functions (5 midline nuclei and 13 bilateral nuclei, for a total of 31 brainstem nuclei) in Illinois Institute of Technology (IIT) space, part of the Brainstem Navigator toolkit v0.9 (<https://www.nitrc.org/projects/brainstemnavigator/>). The brainstem nuclei atlas labels were binarized and thresholded at 35%. The list of these nuclei is as follows: median raphe nucleus (MnR), periaqueductal gray (PAG), substantia nigra-subregion 1 (SN1), substantia nigra-subregion 2 (SN2), red nucleus-subregion 1 (RN1), red nucleus-subregion 2 (RN2), mesencephalic reticular formation (mRt), cuneiform nucleus (CnF), pedunculotegmental nucleus (PTg), isthmus reticular formation (isRt), laterodorsal tegmental nucleus–central gray of the rhombencephalon (LDTg-CGPn), pontine reticular nucleus, oral and caudal part (PnO–PnC), locus coeruleus (LC), subcoeruleus (SubC), inferior olivary nucleus (ION), caudal–rostral linear nucleus of the raphe (CLi–RLi), dorsal raphe (DR), and paramedian raphe nucleus (PMnR; Figure S2). To map the brainstem nuclei atlas from IIT space to native DWI-space, we first built a group-based optimal bivariate FA/ S_0 template from the FA/ S_0 individual images of 19 subjects using an ANTs (Avants et al., 2011) iterative process. We then computed the bivariate diffeomorphic transformations (ANTs) between the group-based optimal bivariate FA/ S_0 template and the IIT FA/ S_0 template (Varentsova et al., 2014). Finally, to map the brainstem nuclei atlas from IIT space to single-subject native DWI space, we concatenated the affine and non-linear transformations from native DWI space to the group-based template with the affine and nonlinear transformations from the group-based template to IIT space and inverted the resulting transformation (see Figure S3).

2.7 | Definition of target regions for tractography computation

The preprocessed MEMPRAGE in native space was the input for the parcellation of the cortex and sub-cortex using FreeSurfer (Destrieux

et al., 2010), resulting in 162 elements that were defined as targets. The accumbens area was excluded from further analysis, and we used instead a basal forebrain label, defined for each brain hemisphere in MNI space, that extended the Harvard-Oxford accumbens atlas label available in FSL (fmrib.ox.ac.uk/fsl/) to also comprise the diagonal band of Broca and substantia innominata (Snider et al., 2019). The hypothalamus in MNI space (Pauli et al., 2018) and subthalamic nucleus in IIT space (Bianciardi et al., 2015) were also used as targets. As additional target regions we used the 31 brainstem regions used as seeds, and 15 other probabilistic brainstem atlas labels (12 bilateral and 3 midline nuclei, for a total of additional 27 nuclei; García-Gomar et al., 2019; Singh et al., 2020, 2021). These labels involved in autonomic, limbic, pain and sensory processing were also binarized and thresholded at 35%.

To map the Freesurfer parcellation from MEMPRAGE space to native DWI-space for each subject, we computed an affine boundary-based transformation (FSL, FLIRT-BBR) between the preprocessed MEMPRAGE and the S_0 image. To map the basal forebrain, and hypothalamic labels from MNI space to native space, we applied the concatenated registrations from MNI to IIT (computed in Bianciardi et al., 2015) and from IIT to single subject diffusion space (through group-based template, see above) using ANTs. To map the subthalamic nucleus and additional 15 brainstem nuclei targets from IIT to native space, we used the same procedure as for the 18 brainstem nuclei seed regions.

2.8 | Tractography computation on 7 T data

We performed probabilistic tractography on 7 Tesla preprocessed data using MRtrix3 (<https://www.mrtrix.org>) iFOD2 algorithm (Tournier et al., 2010) based on constrained spherical deconvolution (Tournier et al., 2007) using the following parameters: 90° maximum angle between successive steps, 0.07 cut-off and 1-mm minimum streamline-length. For each seed-mask, we propagated 100,000 streamlines, and, for each pair of seed-target masks we computed a “structural-connectivity-index” (range: [0 to 1]) equal to the fraction of streamlines propagated from the seed reaching the target mask. We ran the Kolmogorov–Smirnov normality test, which indicated that data did not follow a normal distribution. Therefore, a Wilcoxon test was performed on the connectivity-index values. Then, we corrected the statistics for multiple comparisons using a false discovery rate (FDR) correction. Significant values ($p < .0005$ FDR corrected) were displayed with a 2D circular connectome (Irimia et al., 2012). Further, for display purposes, we computed the average group tract density of each seed mask in IIT space using the coregistrations described above and we performed a Wilcoxon signed rank test using Matlab.

2.9 | 3 T data preprocessing and tractography computation

Diffusion weighted images were processed using a similar pipeline to the one used for the 7 Tesla data (Figure S3). We evaluated the

replicability of 7 Tesla results on 3 Tesla data by computing the correlation coefficient between the correlation matrices averaged across subjects (3 Tesla vs. 7 Tesla). Significance was assessed at $p < .05$. The percentage of common links was also evaluated at different statistical thresholds.

2.10 | Graph analysis and laterality index

Graph Theoretical Network analysis (GRETNA) Matlab toolbox (<http://www.nitrc.org/projects/gretna/>; Wang, Yau, et al., 2015) was used to perform graph analysis. For each seed, the degree centrality and normalized nodal participation coefficient nodal measures were computed. For the latter, we subdivided the network into seven different communities as follows: seeds, brainstem targets, subcortical targets, and then occipital, temporal, frontal, and parietal cortical targets. Note that to perform graph analysis a square connectivity matrix is needed; in the present work, to perform GRETNA analysis, the rectangular connectivity matrix (of size: 27 seeds \times 227 targets) was zero padded (to a matrix size: 227 seeds \times 227 targets); thus, we were able to compute only two nodal measures, the degree centrality and the normalized nodal participation coefficient, which only depend on the seed to target connectivity values (computed in this study) and are independent of the non-seeds to targets connectivity values (zero-padded as described above). Other nodal measures depending on the overall values of the full square matrix (Rubinov & Sporns, 2010) (such as shortest path length, clustering coefficient, local efficiency, and betweenness centrality) were not computed. For each bilateral seed, we also computed a laterality index using Matlab. This index was defined as the difference between the binarized connectome of the left seed and the mirrored value of the right seed, divided by the number of active links. The laterality index ranged between 0% (perfectly symmetric connectivity of the left and right seed) and 100% (perfectly asymmetric connectivity).

2.11 | Diagram generation

We generated schematic diagrams graphically displaying the connectivity of arousal brainstem nuclei and motor brainstem nuclei. We used as nodes the brainstem nuclei grouped according to their involvement in arousal (Lu, 2006; Saper et al., 2001, 2010) and motor (Benarroch, 2012; Cacciola, Bertino, et al., 2019; Cacciola, Milardi, et al., 2019; French & Muthusamy, 2018; Merel et al., 2019) functions, as well as subcortical and cortical structures known to participate in these functions from a system neuroscience perspective. The thickness of lines expressing links between nodes reflects structural connectivity values, after averaging out the connectivity strength of left and right connectivity values for left and right nuclei and of node subregions, to yield a single connectivity value for each couple of nodes. To assess the significance of connectivity we used the same threshold as in the circular plots ($p < .0005$ FDR corrected).

3 | RESULTS

We display the quality of the coregistration of each single-subject fractional anisotropy (FA) image to the IIT template in Figure S4.

In Figures 2–11, we show the structural connectivity results of 31 arousal and motor brainstem nuclei labels used as seeds (18 if we merge left and right seeds) with 227 cortical and subcortical targets (which we refer to as “brain”, i.e., whole brain). Out of these 227 brain regions, 58 are localized within the brainstem (which we refer to as “brainstem”), while the other 169 regions (which we refer to as “rest of the brain”) have been grouped into 21 “subcortical” and 148 “cortical” (further subdivided in lobes) target regions.

In Figure 2a, we display the brainstem seeds to the whole brain connectivity matrix resulting from the analysis of the diffusion 7 Tesla data of 19 subjects ($-\log_{10}[p\text{-value}]$ displayed, FDR corrected at p

$< .0005$). In Figure 2b, we show the 2D circular connectome displaying all significant seeds-to-brain ($p < .0005$ FDR corrected) structural connectivity values. In Figure 2c, nodal graph measures are displayed (degree centrality and normalized nodal participation coefficient). In Figure 2d the laterality index of each seed is displayed. The degree centrality showed that PAG, SN1, SN2, RN1, mRt, CnF, PTg, isRt, LDTg-CGPn, PnO-PnC, LC, SubC, ION, and CLi-RLi are network hubs (i.e., having degree centrality higher than the average degree centrality in the network). The laterality index showed high symmetry for all the bilateral seeds, with slightly decreased symmetry for CnF, LDTg-CGPn, PnO-PnC, and LC.

In Figures 3–11, we display the structural connectome of each individual nucleus on a 2D circular representation ($p < .0005$ FDR corrected). Note that for bilateral nuclei, considering the high symmetry assessed by computing the laterality index, we only show the

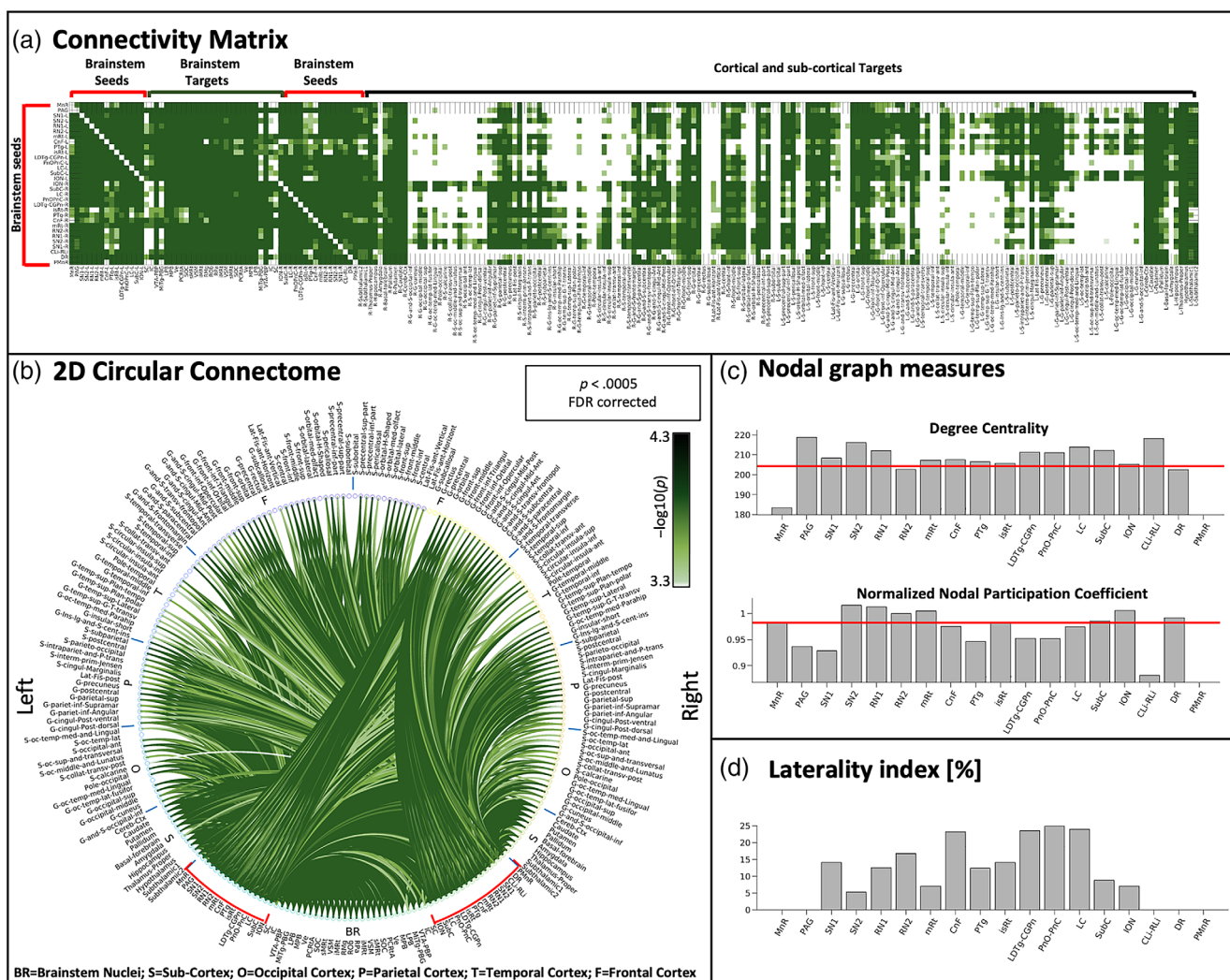


FIGURE 2 Seeds-to-brain connectivity matrix, 2D circular connectome, nodal graph measures and laterality index of all arousal and motor brainstem nuclei. (a) Connectivity matrix of the 31 seeds (15 bilateral seeds and 3 midline seeds) used in the study with the 227 target regions. (b) Circular plot displaying the connectivity matrix values in a 2D representation. In both (a,b) we display the $-\log_{10}(p\text{-value})$ extracted from the group-level region-based analysis of seeds-to-brain structural connectivity ($p < .0005$, FDR corrected). (c) Nodal graph measures, showing the degree centrality, and normalized nodal participation coefficient. (d) Laterality index (ranging from 0% to 100%, i.e., from perfectly symmetric mirrored connectivity of left and right nucleus toward perfectly asymmetric connectivity; list of abbreviations as in Figure 1).

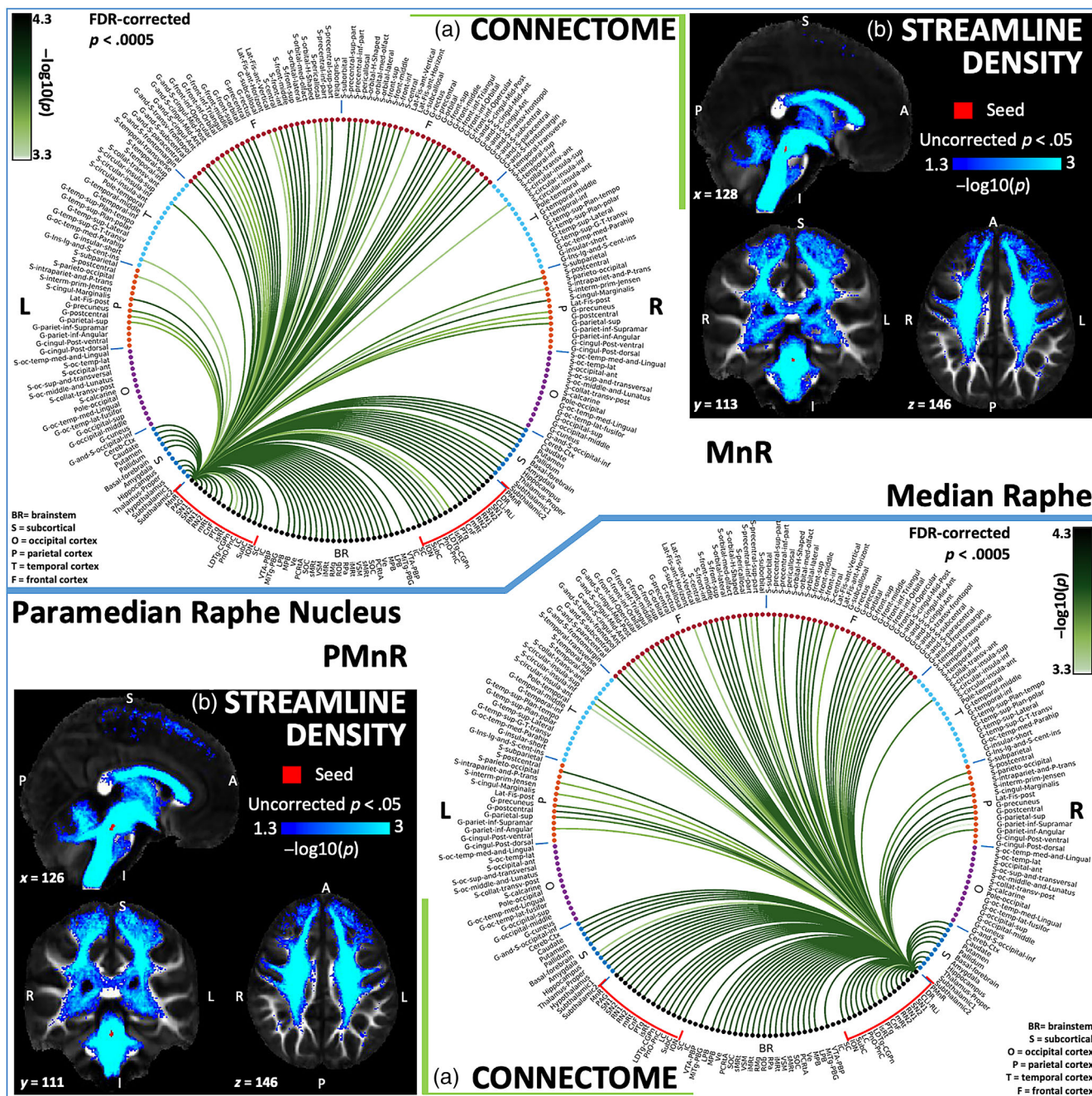


FIGURE 3 Structural connectivity results of median raphe nucleus—MnR (top) and paramedian raphe nucleus—PMnR (bottom). For each nucleus, we display (a) the region-based circular structural connectome ($-\log_{10}(p\text{-value})$, Wilcoxon test, $p < .0005$, FDR corrected), and, for display purposes, (b) the voxel-based streamline density ($-\log_{10}(p\text{-value})$, Wilcoxon test, $p < .05$; list of abbreviations as in Figure 1).

connectome of the left nucleus. For each seed, for display purposes, we also show three orthogonal views of the $-\log_{10}(p\text{-value})$ of the Wilcoxon test across 19 subjects of the voxel-based streamline density resulting from the probabilistic tractography computation.

MnR and PMnR showed strong connectivity with structures involved in arousal, such as the basal forebrain (bilaterally), hypothalamus, and thalamus. Also, both nuclei showed predominant bilateral frontal connectivity and sparser parietal connectivity. Of note, these two nuclei showed similar pattern of connectivity toward other

brainstem areas, some of them involved in arousal, such as PAG, SN1, SN2, PTg, LDTg-CGPn, PnO-PnC, LC, and CLi-RLi (Figure 3).

DR and PAG also showed strong connectivity with structures involved in arousal, such as the basal forebrain (bilaterally), hypothalamus, and thalamus. Also, both nuclei showed bilateral frontal cortical connectivity, and PAG showed bilateral parietal cortical connectivity as well. While DR did not show connectivity with the occipital cortex, PAG showed scarce anatomical connectivity with the occipital cortex. Interestingly, and in agreement with arousal mechanisms affecting

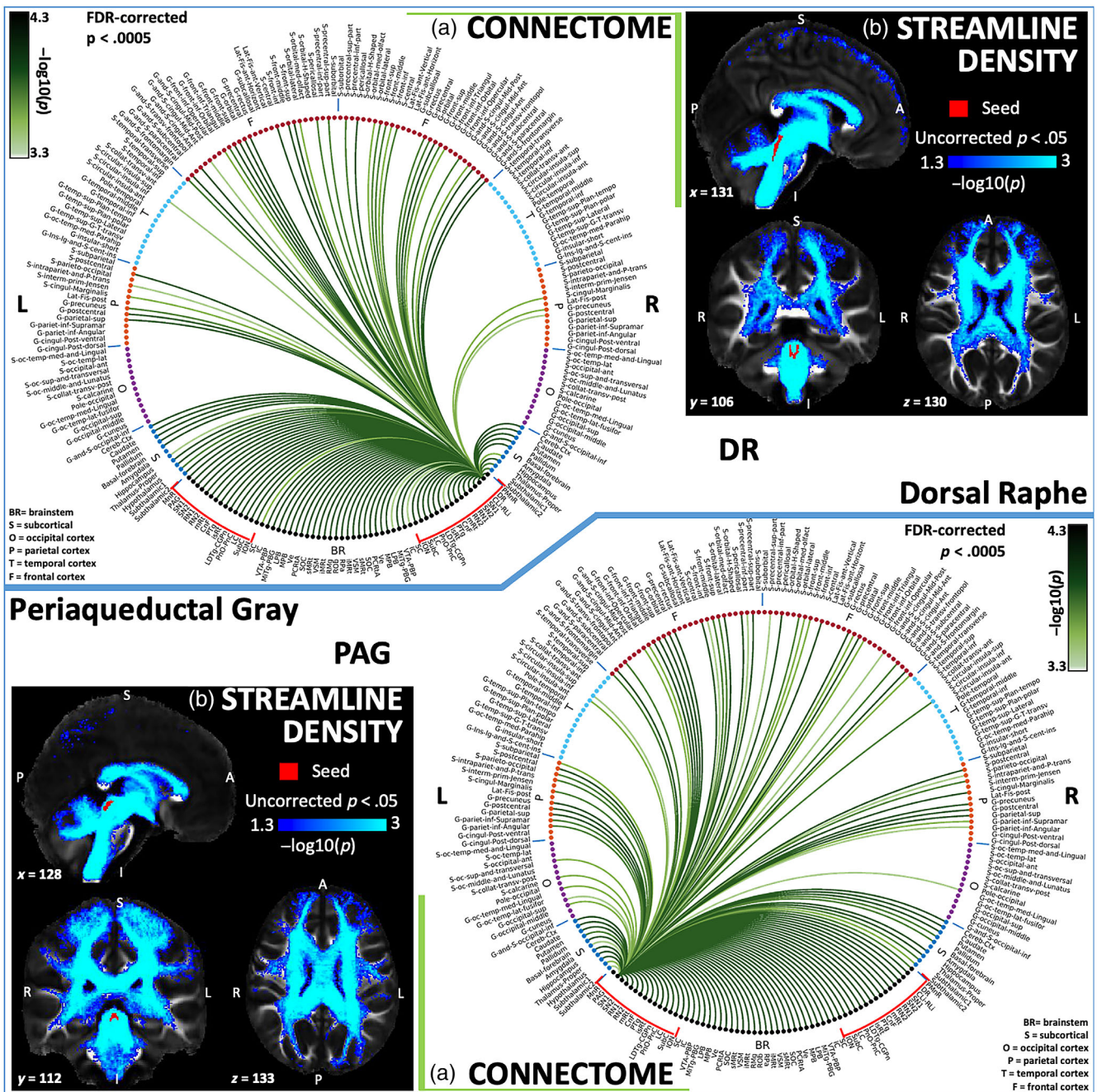


FIGURE 4 Structural connectivity results of dorsal raphe–DR (top) and periaqueductal gray–PAG (bottom). For each nucleus, we display (a) the region-based circular structural connectome ($-\log_{10}(p)$ -value), Wilcoxon test, $p < .0005$, FDR corrected), and, for display purposes, (b) the voxel-based streamline density ($-\log_{10}(p)$ -value), Wilcoxon test, $p < .05$; list of abbreviations as in Figure 1).

widespread areas of the brain, both nuclei displayed strong widespread connectivity toward all the brainstem areas analyzed in the present study, including other arousal centers, motor nuclei, sensory brainstem nuclei (SC, IC, VSM, Ve, SOC), autonomic nuclei (VTA-PBP, LPB, MPB) as well as other raphe nuclei (MnR, RMg, ROB, RPa, and CLi-RLi; Figure 4).

LC showed connectivity toward brainstem midline arousal nuclei (MnR, PAG, CLi-RLi, DR), as well as bilateral brainstem arousal nuclei (SN1, SN2, CnF, PTg LDTg-CGPn, PnO-PnC, SubC, mRt, isRt). Also,

anatomical connectivity toward thalamus, hypothalamus, basal ganglia, cerebellum and bilateral fronto-temporal cortex was found (Figure 5). SubC showed extensive ipsilateral cortical connectivity, including the occipital cortex. It showed strong connectivity towards the other brainstem nuclei, showing lower connectivity strength only with contralateral brainstem sensory nuclei (SC, IC). Interestingly, SubC showed strong bilateral connectivity with inferior and superior medullary reticular formation (iMRt and sMRt, respectively), which contain subregions implicated in REM sleep muscle atonia (Valencia Garcia et al., 2018) (Figure 5).

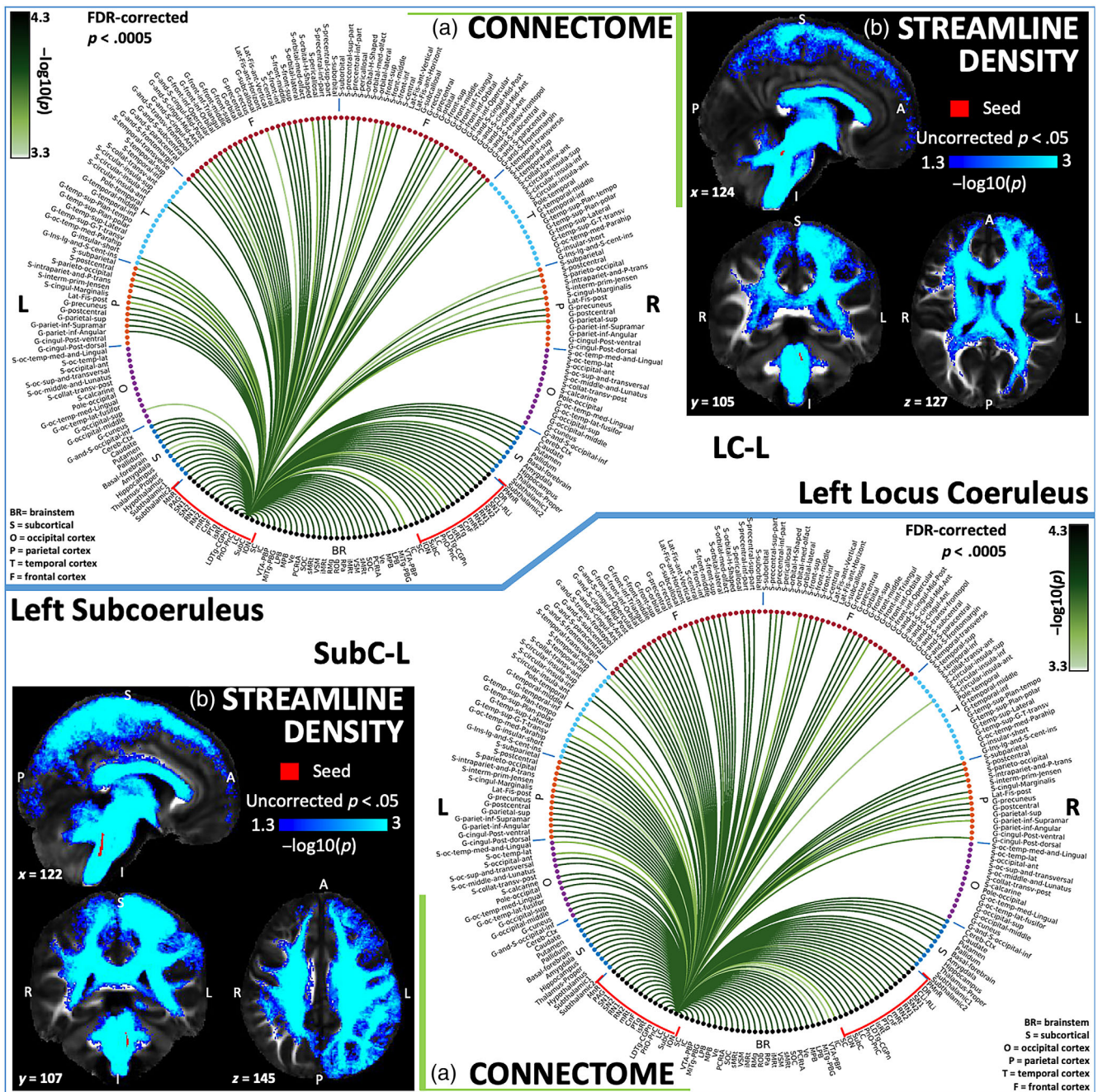


FIGURE 5 Structural connectivity results of locus coeruleus—LC (top) and subcoeruleus—SubC (bottom). For each nucleus, we display (a) the region-based circular structural connectome ($-\log_{10}(p\text{-value})$, Wilcoxon test, $p < .0005$, FDR corrected), and, for display purposes, (b) the voxel-based streamline density ($-\log_{10}(p\text{-value})$, Wilcoxon test, $p < .05$; list of abbreviations as in Figure 1).

LDTg-CGPn showed bilateral fronto-parietal cortical connectivity and ipsilateral insular connectivity, which is in line with its involvement in limbic functions (Mesulam et al., 1989). It showed connectivity with bilateral cerebellum, striatum, hippocampus, thalamus and hypothalamus. Contralateral basal forebrain connectivity was found, while amygdala connectivity was not found at the used p -value. LDTg-CGPn connected to several brainstem nuclei except with MiTg-PBG, and displayed less connectivity strength with sensory brainstem nuclei (SC, IC) (Figure 6). PnO-PnC showed bilateral insular

connectivity, fronto-parietal connectivity, bilateral connectivity with the cerebellum, basal ganglia, amygdala, hippocampus, thalamus, hypothalamus, ipsilateral basal forebrain connectivity, and connectivity with all raphe nuclei, as well toward other arousal, motor, and autonomic brainstem nuclei (Figure 6).

mRt showed expected connectivity with PAG, PnO-PnC, LC, RMg, ION, SC, amygdala, hypothalamus, and cortex. It also showed connectivity to both subregions of SN and RN, and to other brainstem sensory and motor nuclei (Figure 7). While there exists scarce

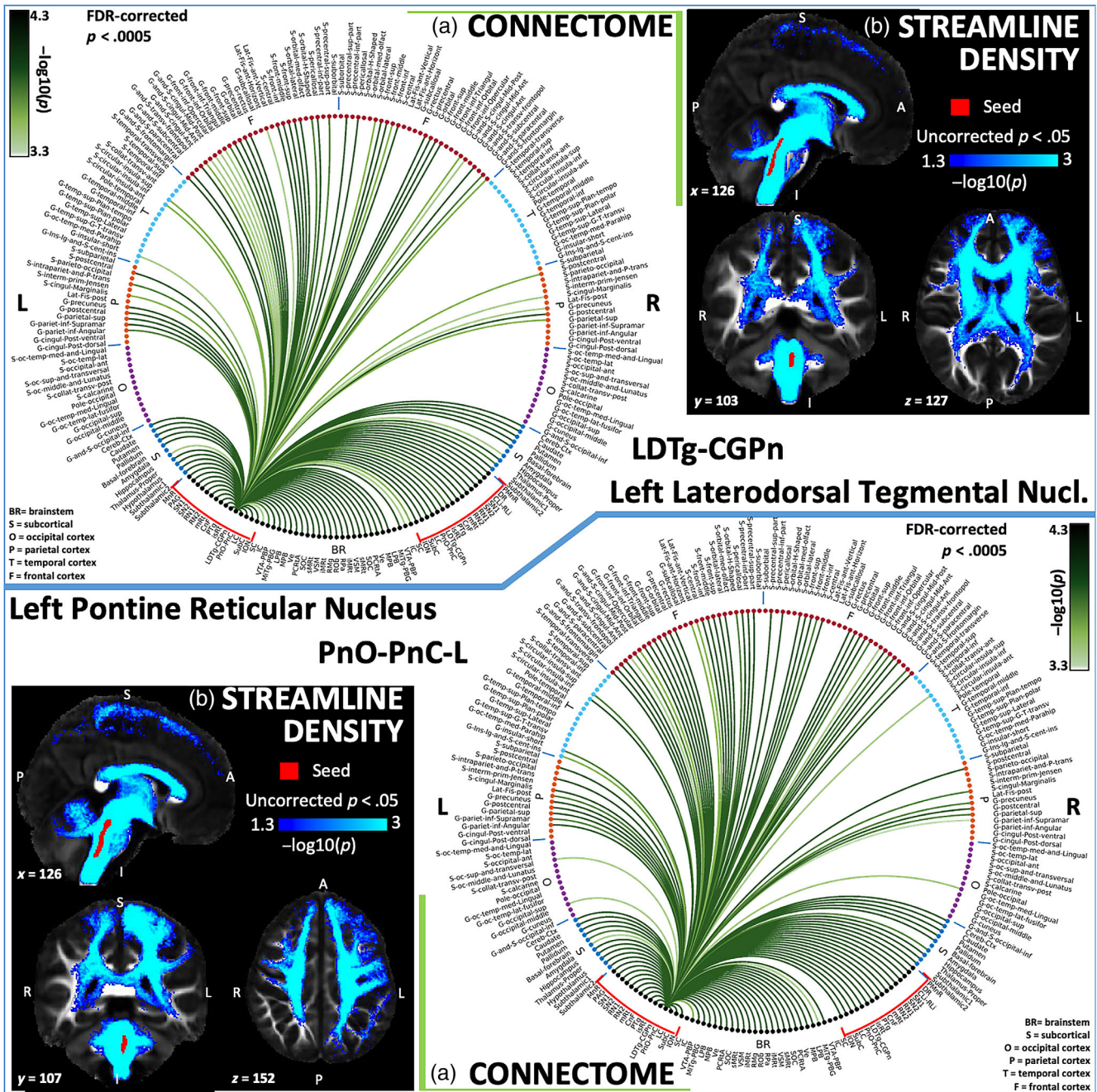


FIGURE 6 Structural connectivity results of laterodorsal tegmental nucleus-central gray of the rhombencephalon-LDTg-CGPn (top), and pontine reticular nucleus, oral part-pontine reticular nucleus caudal part-PnO-PnC (bottom). For each nucleus, we display (a) the region-based circular structural connectome ($-\log_{10}(p)$ -value, Wilcoxon test, $p < .0005$, FDR corrected), and, for display purposes, (b) the voxel-based streamline density ($-\log_{10}(p)$ -value, Wilcoxon test, $p < .05$; list of abbreviations as in Figure 1).

literature of isRt, our results showed a vast brain anatomical connectivity of this nucleus. It showed different degrees of connectivity with different brainstem and cortical areas, stronger ipsilateral connectivity, and weaker connectivity with the contralateral medullary areas (SOC, PCRtA, ION) and pontine areas (LC, PTg) (Figure 7).

PTg and CnF are part of the mesencephalic locomotor region; they showed strong expected connectivity toward other motor brainstem nuclei such as SN1, SN2, RN1, RN2, as well as among

themselves. PTg showed greater connectivity toward cortical and subcortical targets compared with CnF. Both nuclei showed cortical connectivity toward primary motor areas, cerebellum and striatum (Figure 8). Both nuclei showed anatomical connectivity with brainstem arousal nuclei (PAG, CLi-Rli, DR, LDTg-CGPn, and LC), although CnF did not show connectivity with MnR at the used p -value.

We found anatomical connectivity of both SN subregions toward motor and premotor cortical bilateral areas, cerebellum,

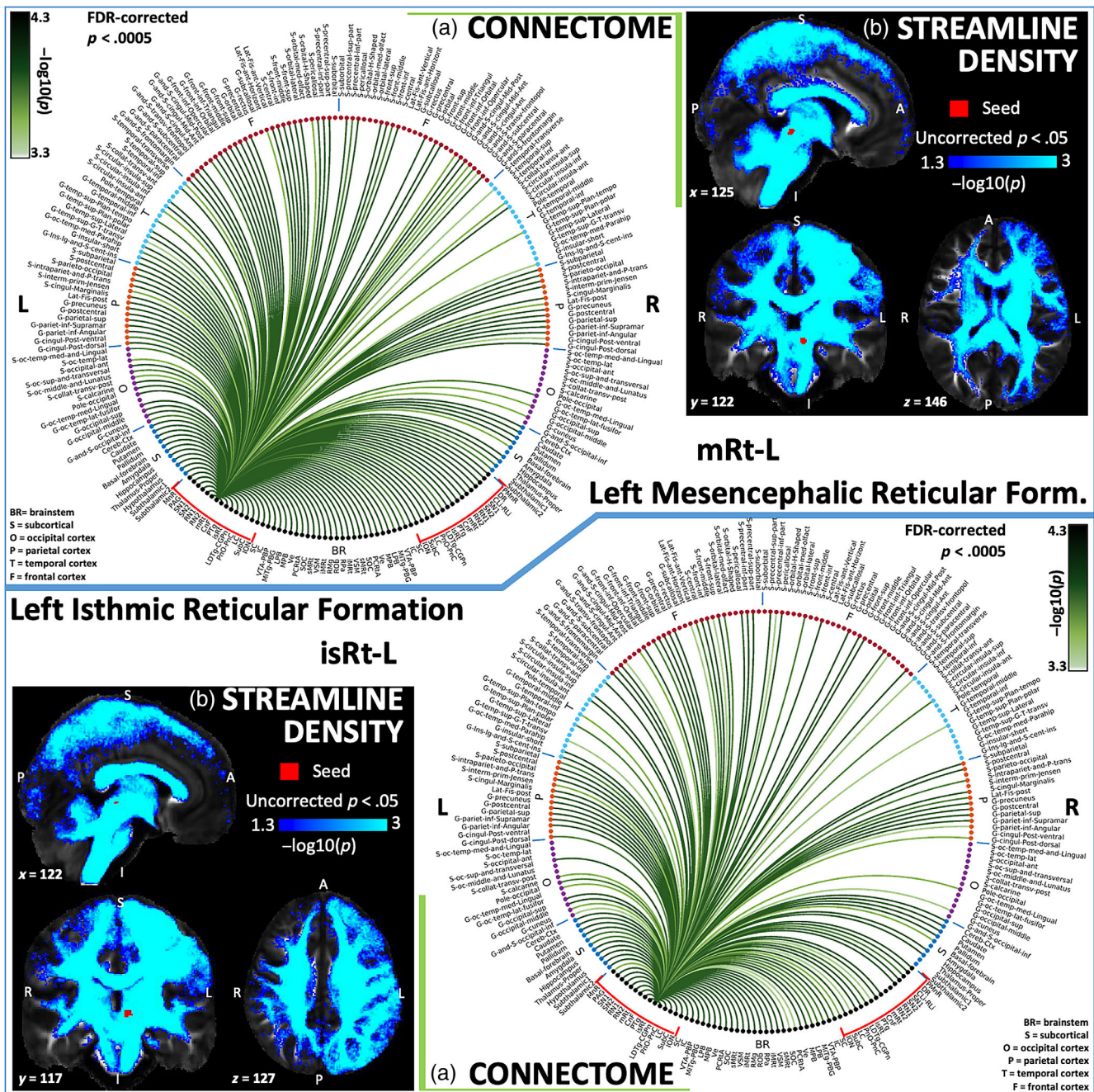


FIGURE 7 Structural connectivity results of mesencephalic reticular formation—mRt (top) and isthmic reticular formation—isRt (bottom). For each nucleus, we display (a) the region-based circular structural connectome ($-\log_{10}(p)$ -value), Wilcoxon test, $p < .0005$, FDR corrected), and, for display purposes, (b) the voxel-based streamline density ($-\log_{10}(p)$ -value), Wilcoxon test, $p < .05$; list of abbreviations as in Figure 1).

striatum, and motor brainstem nuclei (RN1, RN2, contralateral SN, PTg, CnF). Interestingly, we found amygdala connectivity just with the ipsilateral SN2, compatible with substantia nigra pars compacta. Beyond its classical motor function, recent studies showed that SN is also implicated in arousal, reward, and attention (Lee, 2006; Redgrave et al., 2011; Zhang et al., 2017). In line with this broader functionality of SN, we found both subregions to have a widespread connectivity towards cortical and subcortical areas involved in these functions (raphe nuclei, PAG, VTA-PBP, isRt, mRt, SubC,

ION, MiTg-PBG, LPB, MPB, Ve, PCRtA, SOC, sMRt, VSM, iMRt; Figure 9).

CLI-RLI showed bilateral cortical frontal connectivity, and bilateral connectivity to the cerebellum, striatum, thalamus, subthalamus, raphe nuclei, SN1, SN2, RN1, RN2, mRt, CnF, isRt, LDTg-CGPh, PnO-PnC, LC, SubC, ION, VTA-PBP, LPB, MPB, Ve, PCRtA, SOC, sMRt, VSM, iMRt, RMg, ROb, and RPa, as well as to left PTg, left IC, and left MiTg-PBG (Figure 10). ION showed connectivity toward bilateral fronto-parietal cortex, and ipsilateral temporal and occipital cortex. It

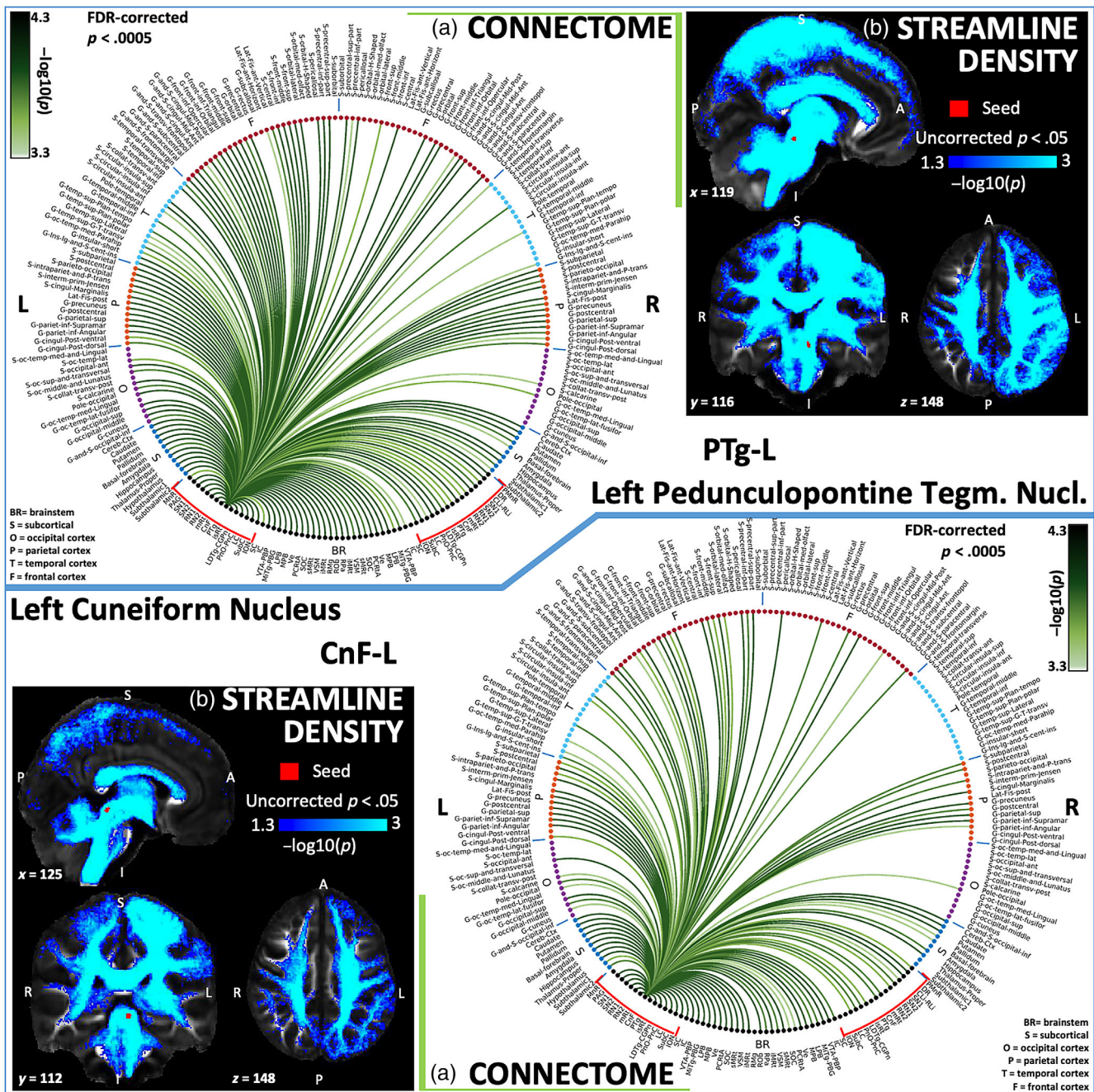


FIGURE 8 Structural connectivity results of pedunculopontine tegmental nucleus—PTg (top) and cuneiform nucleus—CnF (bottom). For each nucleus, we display (a) the region-based circular structural connectome ($-\log_{10}(p)$ -value), Wilcoxon test, $p < .0005$, FDR corrected), and, for display purposes, (b) the voxel-based streamline density ($-\log_{10}(p)$ -value), Wilcoxon test, $p < .05$; list of abbreviations as in Figure 1).

also displayed connectivity toward subcortical motor areas such as bilateral cerebellum, striatum and thalamus. ION showed a predominantly ipsilateral connectivity with PTg, isRt, SN, IC, and LPB, while it showed a bilateral connectivity with the other brainstem nuclei (Figure 10).

Both RN subregions had a similar widespread bilateral frontoparietal cortical connectivity, and ipsilateral temporal and sparse occipital connectivity. RN1 as well as RN2 showed similar connectivity pattern toward subcortical regions (such as ION, cerebellar

cortex, caudate, putamen, pallidum, thalamus, both subregions of the subthalamic nucleus, raphe nuclei, PAG, SN1, SN2, mRt, ipsilateral CnF, PTg, isRt, LDTg-CGPn, PnO-PnC, LC, SubC, ION, ipsilateral SC and IC, VTA-PBP, ipsilateral MiTg-PBG, ipsilateral LPB, MPB, Ve, PCrTA, SOC, sMRt, VSM, iMRt, RMg, Rob, and RPa; Figure 11).

Comparison of the structural connectivity results at 7 Tesla and 3 Tesla is shown in Figure 12 (to quantitative compare 7 Tesla and 3 Tesla images see Figure S5). The association computed on

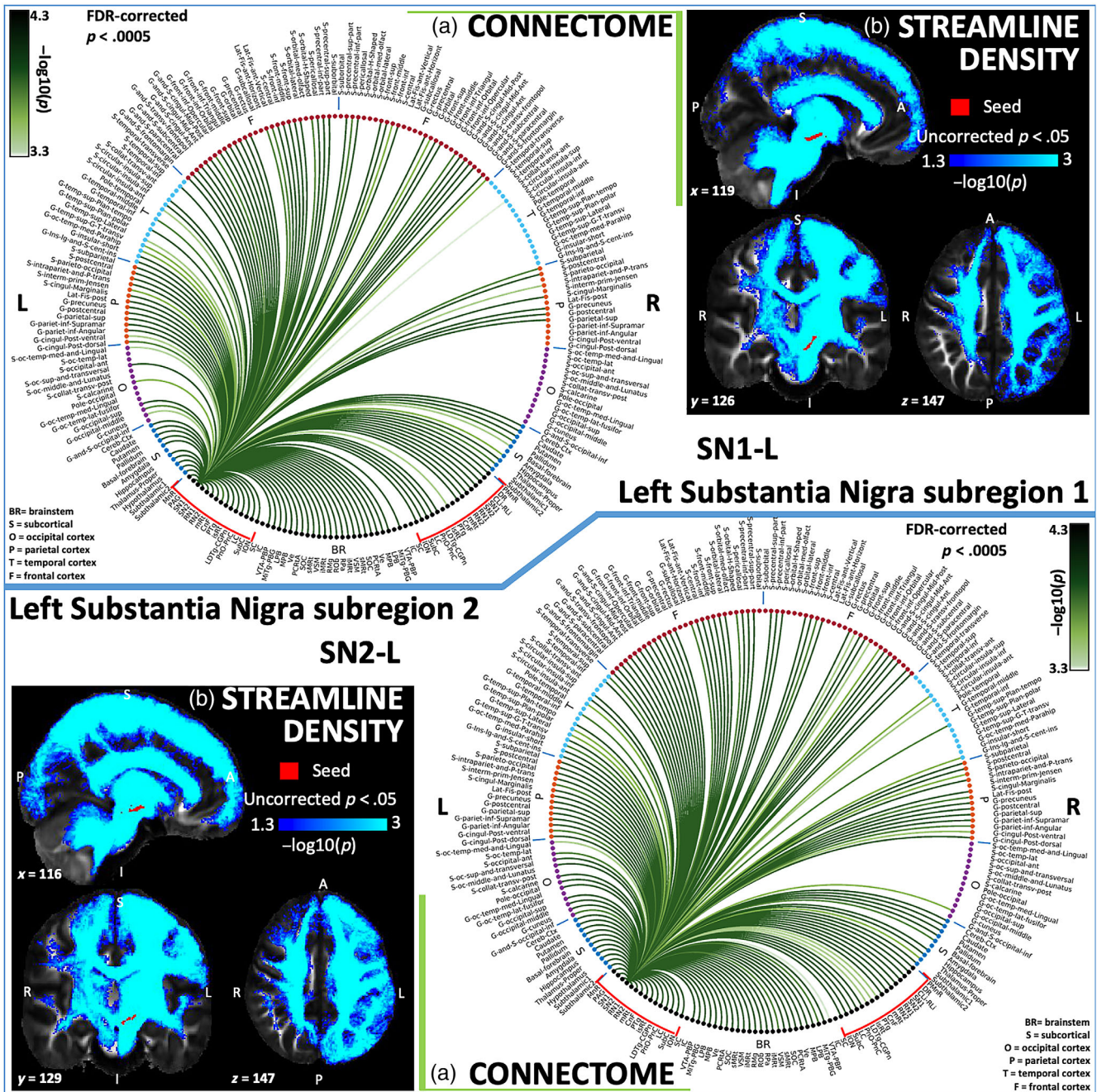


FIGURE 9 Structural connectivity results of substantia nigra subregion 1—SN1 (top) and substantia nigra subregion 2—SN2 (bottom). For each nucleus, we display a) the region-based circular structural connectome ($-\log_{10}(p\text{-value})$, Wilcoxon test, $p < .0005$, FDR corrected), and, for display purposes, (b) the voxel-based streamline density ($-\log_{10}(p\text{-value})$, Wilcoxon test, $p < .05$; list of abbreviations as in Figure 1).

connectivity matrices for seeds-to-brainstem was $r = .55$ and it decreased on seeds-to-the rest of the brain (cortex/subcortex) to $r = .50$. In Figure 12b we show that the percentage of common links between 7 Tesla and 3 Tesla data decreased with increasing the statistical FDR-corrected threshold.

In Figure 13, we display the diagrams of the arousal (top panel) and motor (bottom panel) nodes, with links reflecting the in vivo human structural connectivity values obtained in our analysis. Interestingly, all the brainstem arousal nuclei displayed connectivity with

the thalamus, hypothalamus and among themselves. Brainstem motor nuclei displayed connectivity with the basal ganglia and cerebellar cortex.

4 | DISCUSSION

We investigated the in vivo structural connectivity of arousal and motor brainstem nuclei using a novel in vivo human probabilistic

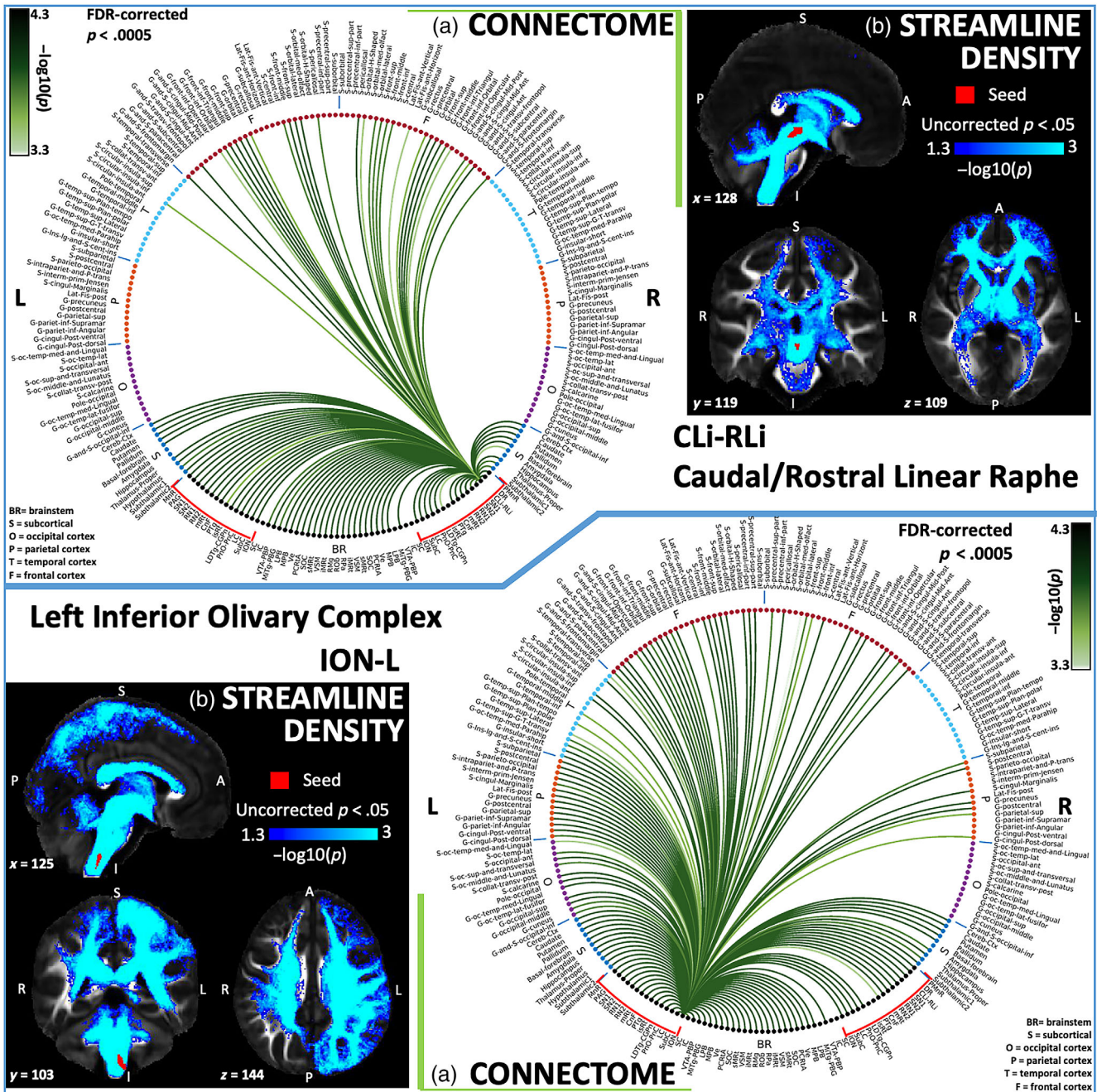


FIGURE 10 Structural connectivity results of caudal–rostral linear raphe–CLI-RLi (top) and inferior olivary complex–ION (bottom). For each nucleus, we display (a) the region-based circular structural connectome ($-\log_{10}(p)$ -value), Wilcoxon test, $p < .0005$, FDR corrected), and, for display purposes, (b) the voxel-based streamline density ($-\log_{10}(p)$ -value), Wilcoxon test, $p < .05$; list of abbreviations as in Figure 1).

structural atlas of these nuclei, and advanced (at 7 Tesla) and conventional (at 3 Tesla) DWIs. First, we discuss the topological properties of the arousal and motor networks based on the graph analysis results and diagram generation. Then, we discuss the findings of the structural connectomes for each brainstem nucleus used as seed, either involved in arousal, motor or both functions. Finally, we discuss the possible impact and limitations of this study.

4.1 | Topological properties of the arousal and motor circuits

We built the circuit diagrams of arousal and motor nodes to validate the human structural connectivity results by summarizing resulting links among nuclei and brain regions that are expected to compose a specific network, defined based on animal and previous human findings.

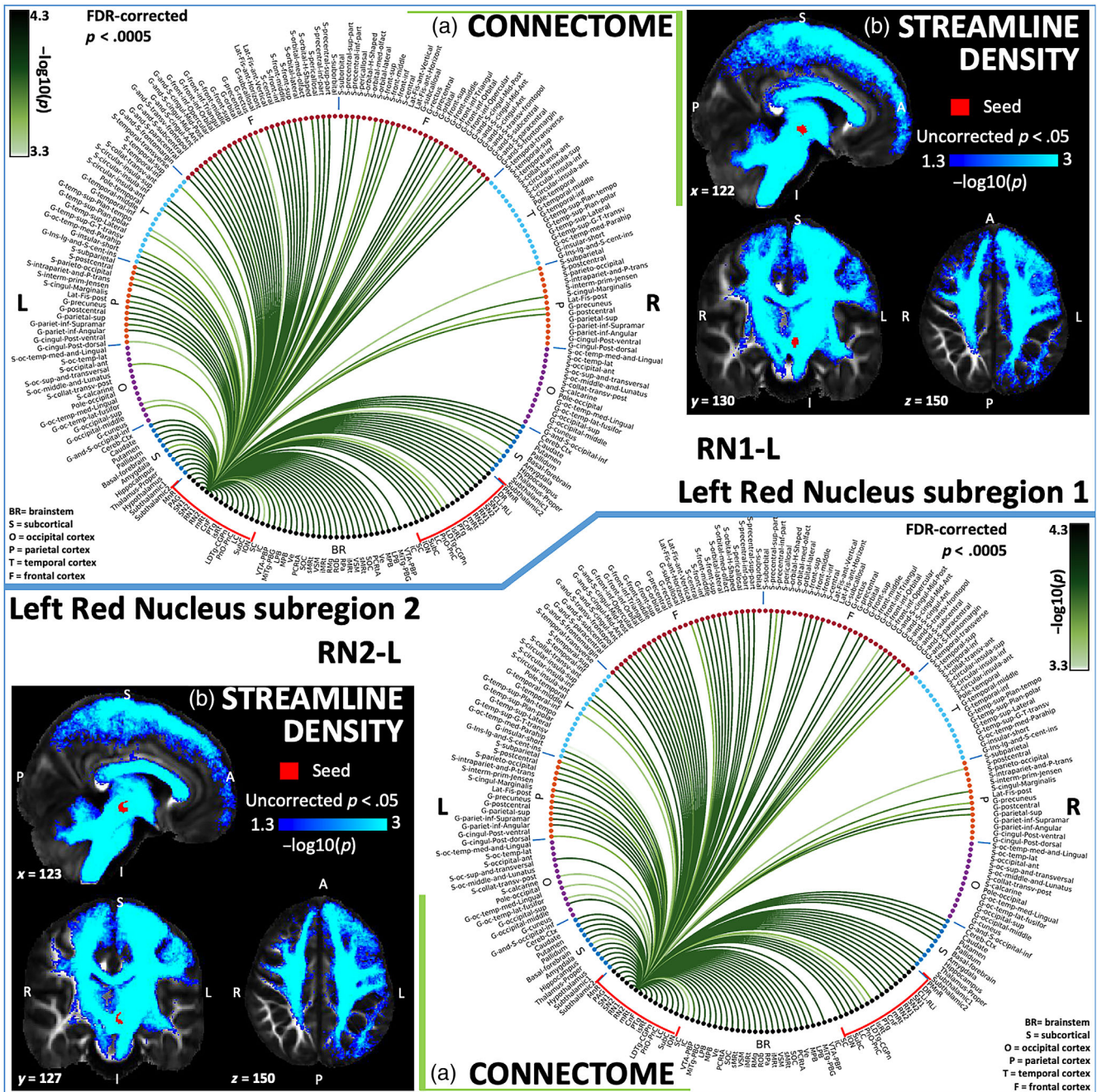


FIGURE 11 Structural connectivity results of red nucleus subregion 1—RN1 (top) and red nucleus subregion 2—RN2 (bottom). For each nucleus, we display (a) the region-based circular structural connectome ($-\log_{10}(p\text{-value})$, Wilcoxon test, $p < .0005$, FDR corrected), and, for display purposes, (b) the voxel-based streamline density ($-\log_{10}(p\text{-value})$, Wilcoxon test, $p < .05$; list of abbreviations as in Figure 1).

The arousal circuit diagram in Figure 13 (top panel) displayed high structural connectivity of brainstem arousal nodes with the thalamus, hypothalamus, basal forebrain, frontal cortex, and among themselves, in agreement with previous literature as shown in Figure 1. The presence of parallel connectivity pathways originating from arousal brainstem nuclei and the high interconnectivity of these nuclei suggest the possible presence of redundant arousal mechanisms in humans. This might be useful to understand,

diagnose or treat disorders associated to impaired arousal (e.g., disorders of consciousness and sleep disorders). Recent research on coma patients recovering consciousness within 6 months from the traumatic event identified the presence of microbleeds in multiple arousal brainstem nuclei, yet no single arousal nucleus was commonly affected across the sample (Bianciardi et al., 2021). The underlying strong anatomical interconnectivity of the arousal circuit shown in the present study might

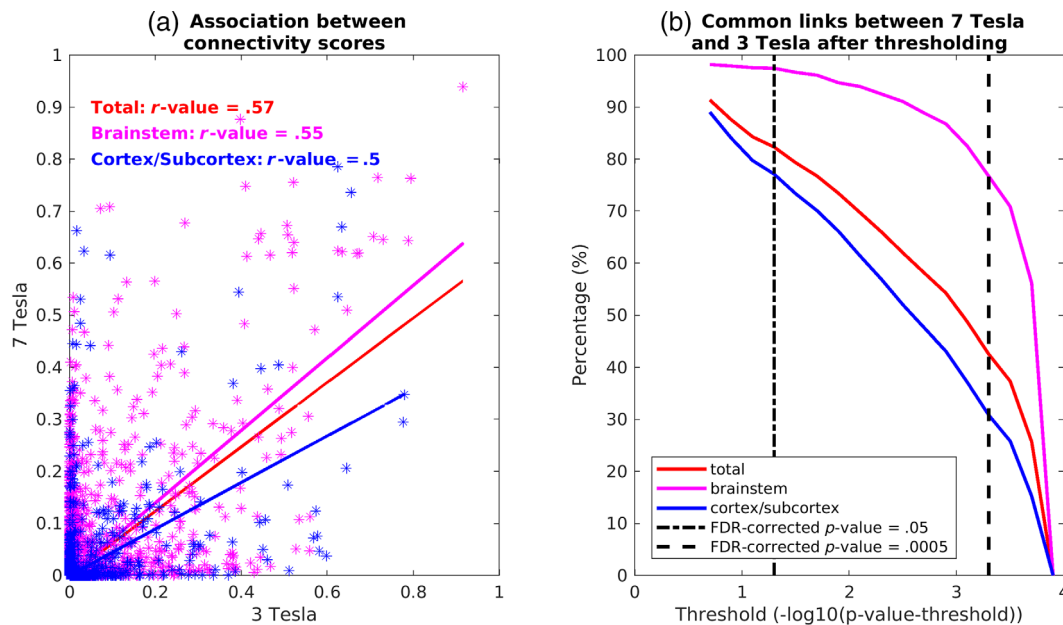


FIGURE 12 Translatability of 7 Tesla results in a conventional dataset acquired at 3 Tesla. (a) Association values between the structural connectivity scores obtained at 7 Tesla and 3 Tesla for whole brain-total (in red), brainstem only targets (in magenta), and cortical/subcortical (other than brainstem) targets (in blue); (b) percentage links in common between 7 Tesla versus 3 Tesla results found in the whole brain-total, brainstem, and cortex/subcortex for different statistical thresholds (the black vertical lines indicate FDR-corrected p -values of .05 and .0005).

provide a neuroanatomical framework for the resiliency of arousal mechanisms shown in Bianciardi et al. (2021).

In Figure 13 (bottom panel) we displayed the motor circuit diagram, which showed high interconnectivity between the basal ganglia, frontal motor cortex, cerebellum and brainstem nuclei implied in motor control, such as RN, SN, ION, PTg, and CnF. This is in line with the literature on the central motor control, as shown in Figure 1 (Boeve et al., 2007; Manto et al., 2012; Valencia Garcia et al., 2018). Specifically, subcortical structures such as basal ganglia are involved in direct and indirect pathways implicated with the selection and performance of movements. Furthermore, basal ganglia play an important role in reward, reinforcement, and habit formation. The cerebellum is involved in sensorimotor control and is deeply related with the adjustment of movements through trial and error (Manto et al., 2012), which closely relates to its projections to the ION and motor cortex observed in this study. Instead, SubC and sMRt (containing the gigantocellular reticular nuclei) are involved in REM sleep atonia (Boeve et al., 2007; Valencia Garcia et al., 2018).

Taken together, the system neuroscience findings depicted in the circuit diagrams (Figure 13) agree with the nodal graph analysis of the brainstem nuclei. Indeed, the latter (Figure 2) showed that 14 out of 18 investigated brainstem nuclei had a degree centrality higher than the average. This indicates high information exchange ability in the network, in line with the information displayed in the circuit diagrams. Moreover, the nodes that contributed the most to the intercommunity communication, as evinced from the normalized nodal participation coefficient, were: MnR, SN and RN (the latter two with their corresponding subregions), SubC, ION, and DR.

4.2 | Structural connectivity of individual brainstem nuclei

The structural connectome of the serotonergic *median raphe nucleus* (MnR) and *paramedian raphe nucleus* (PMnR) showed bilateral connectivity with the basal forebrain and hypothalamus in agreement with previous mice reports (Liu et al., 2012). Both nuclei also showed expected connectivity with other raphe nuclei such as CLi-RLi and DR (Molliver, 1987). Interestingly, as previously reported in animal studies, MnR showed structural connectivity with the hippocampus although only in the right hemisphere. This might be related to its roles in modulation of hippocampal activity during sleep and in consolidation of fear memory (Vertes, 2010; Wang, Wang, et al., 2015), with the possible involvement for the second task also of the prefrontal cortex and thalamocortical connections. In agreement with previous research, MnR showed connectivity predominantly to the frontal cortex, striatum, thalamus, cerebellum, and smaller cortical regions widely distributed (Molliver, 1987) in the parietal lobe, with sparser and weaker connections in the temporal lobe. Due to its widespread connectivity and serotonergic neurotransmission, MnR is considered to be part of the neuromodulatory system (Olszewski & Baxter, 2014). In agreement with the literature (Molliver, 1987; Vertes, 2010), neither MnR nor PMnR demonstrated direct connectivity with the amygdala. This finding might be in line with recent optogenetic findings showing that stimulation of MnR can generate remote but not immediate fear memory (Balázsi et al., 2017). In contrast, PMnR is a less studied brainstem nucleus; it surrounds MnR, and, although the boundaries of these two nuclei have been well established by finding an AChE-

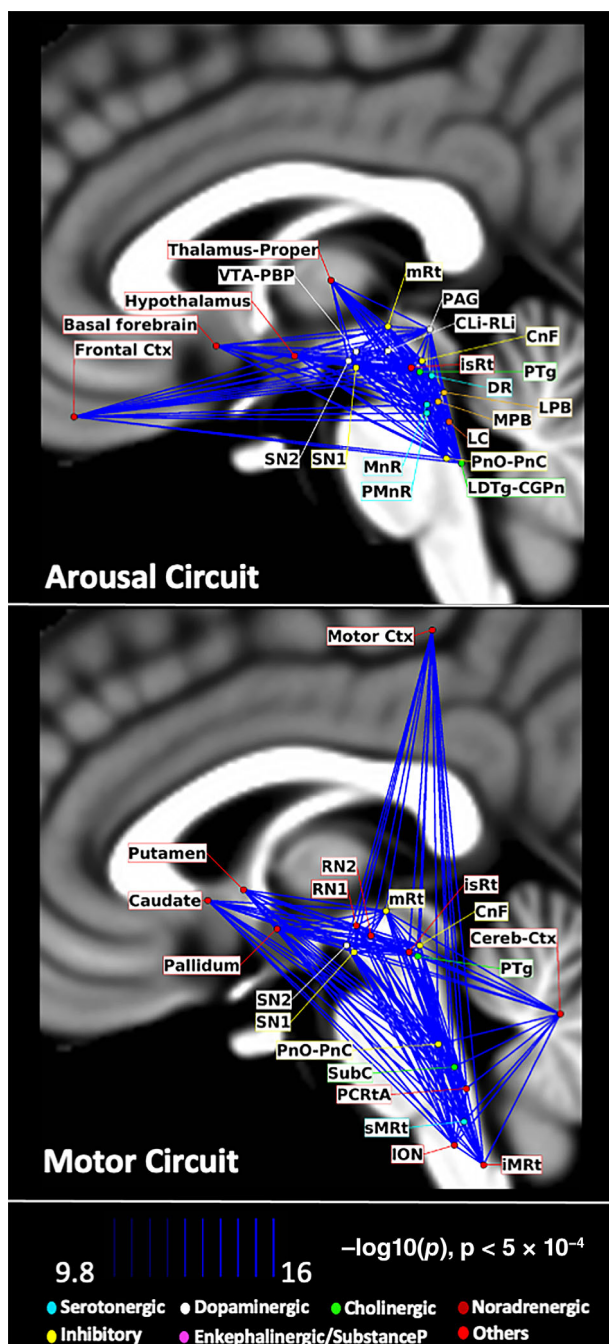


FIGURE 13 Circuit diagram of the arousal (top) and motor (bottom) network derived from probabilistic tractography of 7 Tesla DWI. The arousal brainstem nuclei displayed high structural connectivity with thalamus, hypothalamus, basal forebrain, frontal cortex, and among themselves. The very high interconnectivity of the arousal circuit could indicate the presence of redundant arousal mechanisms. The motor circuit diagram showed connectivity of brainstem nuclei in agreement with the literature (Benarroch, 2012; Cacciola, Bertino, et al., 2019; Cacciola, Milardi, et al., 2019; French & Muthusamy, 2018; Merel et al., 2019), including with the motor cortex, putamen, caudate, pallidum and cerebellar cortex. The brainstem nuclei are color-coded based on the major neurotransmitter released by each region. The thickness of lines between nodes reflects the connectivity strength among them based on the $-\log_{10}(p\text{-value})$ ($p < .0005$, FDR corrected).

positive zone in between the two nuclei (Paxinos et al., 2012), some authors consider it as a subdivision of MnR itself (Olszewski & Baxter, 2014). Our results showed similar pattern of connectivity of these two nuclei, including the lack of connectivity with the amygdala, CnF, visual and auditory relay nuclei (superior and inferior colliculi), MiTg-PBG, meanwhile showing widespread connectivity to other brainstem nuclei (e.g., raphe nuclei) and dense frontal cortical connectivity.

The *dorsal raphe* (DR) contains the largest population of serotonergic cells in the human brainstem (Charara & Parent, 1998). Nonetheless, it is a very anatomically and neurochemically diverse region, since less than 50% of its neurons are serotonergic and the remaining cells release other neurotransmitters (Huang et al., 2019). Multiple functions have been attributed to this nucleus (such as arousal, sleep-wake cycles, regulation of memory, learning, anxiety related functions, and movement), and it has also been implicated in a variety of behavioral and neurological disorders (e.g., major depressive disorder, bipolar disorder, schizophrenia, and obsessive-compulsive disorder; Huang et al., 2019). In agreement with previous literature and recent anatomical tracing studies (Huang et al., 2019; Olszewski & Baxter, 2014), our results showed that DR has structural connectivity with frontal and prefrontal cortex, striatum, thalamus, accumbens (contained in the basal forebrain area), and other brainstem nuclei like SN1, SN2, PAG, and LC. Although the connectivity of DR with the amygdala has been previously reported (Vertes, 2010), it was not significant in our connectome.

The *periaqueductal gray* (PAG) is an important relay in autonomic cardiovascular control, modulation of pain, and arousal function that has been involved in REM sleep and non-REM sleep stages (Benarroch, 2012; Paxinos et al., 2012). We found structural connectivity of the PAG with hypothalamus: recent studies using diffusion-based tractography in humans showed changes in the microstructural properties of this tract, which correlate with pain level in veteran patients with chronic pain (Zhang et al., 2020). As in the current study, animal studies report connectivity between PAG and LC, pontine reticular formation (PnO-PnC in this study), medulla dorsolateral to the pyramids (presumably in the area corresponding to iMRt and PCRtA), SubC, RMg, gigantocellular, and paragigantocellular nuclei (part of sMRt in the present study; Cameron, Khan, Westlund, & Willis, 1995). We also found connectivity between PAG and bilateral cerebellum; interestingly, a recent tractography study has also described this connectivity in humans (Cacciola, Milardi, et al., 2019). Ascending projections previously reported in the structural connectivity of animals (Cameron, Khan, Westlund, Cliffer, & Willis, 1995) were also found in our human connectome, that is, links with the thalamus, hypothalamus, VTA, SN1, SN2, and diagonal band of Broca, which is included in the basal forebrain label in the present study. PAG connectivity with the amygdala and cortical structures such as the medial prefrontal cortex, orbitofrontal cortex, and infralimbic cortex have been involved in networks associated with fear learning and fear conditioning (Watson et al., 2016); this structural connectivity was also present in our connectome, and has been described in animals using invasive tracers (Ferreira et al., 2015), thus validating our results. In

summary, we found that PAG showed a dense connectivity to brainstem regions and sparser, yet specific, connectivity with cortical areas.

The *locus coeruleus* (LC) is a noradrenergic neuromodulator, which modulates the activity of distant brain areas involved in wakefulness, autonomic function, attention, behavioral flexibility, stress response, memory, and cognitive processes (Bari et al., 2020). Despite its small size, this nucleus contains the largest portions of noradrenergic neurons in the mammalian brain (Sharma et al., 2010). It has extensive efferent projections to innervate limbic regions (including the hippocampus) and the whole neocortex, as also visible in the 2D structural connectome plot (Figure 5). In line with our findings, LC projects to the thalamus, hypothalamus, pallidum, VTA, substantia nigra (SN), amygdala, hippocampus, and numerous brainstem nuclei (Bari et al., 2020). The connectivity with amygdala, hippocampus, and VTA might underlie the central role of LC in learning and memory. Interestingly, our results showed only ipsilateral connectivity with the amygdala, while showing bilateral hippocampal connectivity. In line with literature (Olszewski & Baxter, 2014), the following brainstem sensory nuclei displayed anatomical connectivity with LC: the solitary nucleus (included in VSM), PAG, ION, DR, and lateral paragigantocellular nucleus (included within the sMRt label), as well as the cerebellum. The cortical distribution of LC connectivity was widespread, yet with preferential connectivity with the bilateral frontoparietal cortices, in agreement with an extensive study of rat immunocytochemical noradrenaline axon terminals (Séguéla et al., 1990). This connectivity profile is also supported by electroencephalogram (EEG) findings (Berridge & Waterhouse, 2003) where a unilateral LC pharmacological inhibition or excitation produced a bilateral cortical EEG response. LC has also been reported to show histological changes related to aging, as well as neurodegeneration in Alzheimer's disease, Parkinson's disease, sleep disturbances, and psychiatric diseases as depression (Bari et al., 2020; Sharma et al., 2010). Future studies should further explore its connectivity changes related to these conditions.

The nucleus *subcoeruleus* (SubC) is thought to be involved in the generation of REM sleep and of ponto-geniculo-occipital waves (Simon et al., 2012). As visible in our results, we found dense structural connectivity of the SubC with ipsilateral occipital cortex, thalamus, and bilateral frontoparietal connectivity. This connectivity might underlie the characteristic EEG pattern on the occipital lobe during REM sleep (Adamantidis et al., 2019). Previous studies have found decreased signal in this area in Parkinson's disease patients with rapid eye movement sleep behavioral disorder symptoms (García-Lorenzo et al., 2013); thus, SubC might also be involved in non-motor symptoms of Parkinson's disease. In line with literature (Olszewski & Baxter, 2014), we found connectivity of SubC with limbic structures such as the hypothalamus, amygdala and basal forebrain, PAG, pontine reticular formation (PnO-PnC), parabrachial nuclei (MPB, LPB), vestibular nuclei (Ve), and gigantocellular nucleus (Gi, contained within the sMRt label). Crucially, the observed structural connectivity between SubC and sMRt is in line with the key role of SubC in the generation and maintenance of REM sleep muscle atonia (Boeve et al., 2007; Valencia Garcia et al., 2018).

The *laterodorsal tegmental nucleus* (LDTg) is a brainstem cholinergic nucleus, previously described as the most conspicuous and extensive cell group of the rostral brainstem (Mesulam et al., 1989). The cholinergic neurons spread into the *central gray of the rhombencephalon* (CGPn). The LDTg and the PTg provide the major cholinergic innervation to the thalamus, and might be connected with the limbic system (Mesulam et al., 1989). Cornwall et al. studied in rat the LDTg connections using lectin tracers; they obtained vast cortical and subcortical connectivity resembling our results (Cornwall et al., 1990). Specifically, in line with the rodent study (Cornwall et al., 1990), LDTg showed connectivity with the frontal cortex, diagonal band of Broca (within the basal forebrain), hypothalamus, thalamus, VTA, SN, parabrachial nuclei (MPB, LPB), nucleus of the tractus solitary (within VSM), interpeduncular nucleus (within VTA-PBP), infralimbic cortex, cingulate cortex, hippocampal cortex, preoptic areas, SC, ION, MnR, DR, and PTg. Interestingly, the rat study (Cornwall et al., 1990) using invasive tracers did not find any labeling in the central nucleus nor in the bed nucleus of the amygdala; in the present study using non-invasive in vivo fiber tracking in living humans ($p < .0005$ FDR corrected) we also did not find connectivity between LDTg and the amygdala. LDTg has been involved in arousal and emotional arousal under adverse conditions (Bueno et al., 2019); its connectivity with limbic areas (ipsilateral insula and bilateral cingulum) might support its functional role in processing aversive information. In addition, recent optogenetic rodent research has found that direct projections from LDTg to the accumbens play an important role in reward-related behaviors (Coimbra et al., 2019). In line with these findings, in our study we found bilateral connectivity with LDTg and basal forebrain which contains the accumbens.

The *pontine reticular formation nucleus, oral, and caudal part* (PnO-PnC), is involved in conjugate eye movements to the ipsilateral side. The neurons of this nucleus are active during saccades and the quick nystagmus phase, and they are involved with the horizontal gaze center (Robinson et al., 1994). More recent research shows that PnO receives cholinergic inputs from PTg, LC, LDTg, and parabrachial nuclei, and that cholinergic agonist applied to this nucleus can produce long-lasting rapid eye movement sleep with short latency (Rodrigo-Angulo et al., 2005). Interestingly, the connectivity of PnO-PnC to these regions, previously reported in cat, was also observed in our 2D structural connectome in living humans. Despite previous reports in cats showing weaker structural connectivity between PnO and rostral raphe nuclei (Rodrigo-Angulo et al., 2000), our results found strong anatomical connectivity with raphe nuclei (i.e., MnR, PMnR, RMg, DR, CLi-RLi). Future studies might further investigate these results in humans and possibly explain if these changes are related to evolution and variability across species.

The *mesencephalic reticular formation* (mRt) is involved in gaze control and head movements; it controls the head position and eye movements such as saccades, fixation, and vergence, and it has a crucial role in space-time saccades (Graf & Ugolini, 2006; Holstege, 1988). It receives direct connectivity from the subcortical and cortical eye movement centers: SC, frontal eye fields (Huerta et al., 1986; possibly equivalent to FreeSurfer parcellation of G-

frontal-sup, G-frontal-middle, S-frontal-sup, and S-frontal-middle), and supplementary eye fields (Huerta & Kaas, 1990; possibly equivalent to FreeSurfer parcellation of S-precentral-sup-part and G-and-S-paracentral in our connectomes). Notable, we found these connections in our structural connectome. Further, we found connectivity with the ipsilateral amygdala, basal forebrain, hypothalamus, PAG, RMg, LC, and ION in agreement with previous literature (Holstege, 1988), and with its involvement in arousal.

The recently added nucleus of *isthmus reticular formation* (isRt) has been understudied (Paxinos et al., 2012). Based on its anatomical proximity to arousal and motor nuclei and to its similar connectivity profile to PTg we speculate that these two nuclei might have similar functions, also considering that isRt was previously located in a region pertaining to PTg (Paxinos & Mai, 2007). Nevertheless, we found differences between the strength of the connectivity of these two nuclei with other brainstem nuclei (i.e., SC, SOC, PCRtA) and a lack of connection of isRt with the contralateral RN, contralateral subthalamic nucleus and contralateral amygdala. Future studies might help to extend the knowledge of this area and its functions.

The *pedunculotegmental nucleus* (PTg), also known as pedunculopontine nucleus, and the CnF have been grouped together as the mesencephalic (or midbrain) locomotor region (Shik et al., 1966). The function of PTg goes beyond the motor component, to include a possible role in sleep-wake cycles, arousal, attention, learning, and reward (French & Muthusamy, 2018; Garcia-Rill et al., 2019; Stefani et al., 2013). A previous study showed that PTg has a widespread cortical connectivity, with a predominance toward the frontal lobe and specifically with the pre-motor cortex (Muthusamy et al., 2007); reciprocal connectivity with the ipsilateral prefrontal cortex has also been reported (Pahapill, 2000). Our results replicated this previously reported anatomical connectivity; in addition we observed connections of PTg with the primary motor area (compatible with G-precentral and S-precentral-sup-part in our connectomes), supplementary motor area (compatible with G-Front-sup in our connectomes), somatosensory motor area, pre-supplementary, dorsal and ventral premotor cortex, and frontal eye fields in agreement with previous research (French & Muthusamy, 2018; Kuypers & Lawrence, 1967; Matsumura et al., 2000). PTg also showed structural connectivity with subcortical structures such as the basal ganglia, subthalamic nucleus, SN, cerebellum, thalamus, hypothalamus, and numerous brainstem regions. Understanding the anatomical connectivity of this nucleus might give valuable insights to the physiopathology of Parkinson's disease, as well as a deeper understanding of the underlying mechanism of motor and non-motor effects of deep brain stimulation.

The *cuneiform nucleus* (CnF) is involved with locomotor function; recent studies specifically attribute the elicitation of high-speed synchronous-gait locomotion to the glutamatergic neurons of this nucleus (Caggiano et al., 2018), possibly related with escape behavior during locomotion, in close interaction with PTg. Using retrograde trans-synaptic tracing, recent research in rodents found connectivity of CnF with predominantly ipsilateral inputs, with stronger projections from midbrain structures (such as PAG and IC); this study also showed

little input from basal ganglia and sensory-motor and frontal cortices (Caggiano et al., 2018). As expected, previous rodent studies showed that there is high interconnectivity between CnF and PTg with dominant projections going from CnF to PTg, which might modulate PTg activity to slow or alternate locomotion (Caggiano et al., 2018). Interestingly, the abovementioned invasive tracing studies are in line with our findings; specifically, we found a decreased connectivity of the CnF with the cortex compared with PTg, and, as in rodents, CnF showed connectivity with PAG and bilateral IC. We also found for CnF and PTg a stronger ipsilateral cortical and subcortical connectivity than the contralateral one. Future studies might analyze in detail the interactions of CnF with cerebellar structures also involved in motor and cognitive functions. In contrast to what has been reported in the literature, we did not find anatomical connectivity of the CnF with the RMg (Beitz, 1982), although we found connectivity of CnF with other raphe structures (PMnR, DR, CLi-RLi, ROb, and RPa). Changes in CnF structural connectivity have been found in epilepsy and in chronic fatigue syndrome (Barnden et al., 2019; Englot et al., 2018). Overall, the connectivity of PTg seems to encompass additional brain areas compared with the CnF connectivity; this is in line with recent research postulating that neurosurgical treatment for motor disorders might be better targeted when directed to CnF due to its less diffuse brain connectivity (Chang et al., 2020).

In this work, we investigated the connectivity of two subregions of SN, namely the *substantia nigra-subregion1* (SN1), compatible with pars reticulata, and *substantia nigra-subregion2* (SN2), compatible with pars compacta. SN is involved in arousal, reward, attention, and motor functions (Lee, 2006; Redgrave et al., 2011; Zhang et al., 2017). According to its projections, previous reports found three territories within this dopaminergic nucleus: limbic, cognitive, and motor (Zhang et al., 2017). Based on its functions, the structural connectivity of this nucleus is highly widespread. The SN has cortical and subcortical structural connectivity with ventral striatum, prefrontal cortex, cingulum, thalamus, SC, amygdala, hippocampus, subthalamic nucleus, brainstem structures such as the PTg, VTA (Lee, 2006; Mena-Segovia et al., 2004), and raphe nuclei (Zhang et al., 2017). Interestingly, for both subregions, we found all the above mentioned expected anatomical connectivity in our data (see the 2D connectomes plots—Figure 9), except for the links of SN1 toward the amygdala and SC, while SN2 showed anatomical connectivity with the ipsilateral amygdala. This link would be relevant to verify a recently proposed progression model of alpha-synuclein accumulation (Borghammer, 2021), which postulates the existence of a brain-first Parkinson's disease subtype based on the ipsilateral spread of the misfolded protein from the amygdala toward ipsilateral SN. This connectivity is visible in our connectome plot of SN2 (not present when looking SN1 to amygdala structural connectome), corresponding to the pars compacta that interestingly is the furthestmost affected subregion in this disease. Despite a research study in primates showing connectivity of SN with SC (Parent et al., 1983), in the present study we did not find this connection. Previous studies in rodents have also shown different attention behavior in rats when lesioning the pathway of this nucleus with the ipsilateral versus the contralateral amygdala (Stefani et al., 2013).

Nevertheless, we did not find a significant contralateral anatomical connectivity of SN subregions with the amygdala.

The *caudal-rostral linear raphe (CLi-RLi)*, belonging to the rostral serotonergic group of the raphe nuclei, showed bilateral connectivity with the frontal cortex. In line with previous studies, we found connectivity with the basal forebrain (Hornung, 2003), basal ganglia, hypothalamus, VTA-PBP, and SN (Olszewski & Baxter, 2014), while we did not find anatomical connectivity with the amygdala. RLi is a midline component of the dopaminergic VTA, and has been related with reward and motivation (Flores et al., 2006). Previous invasive research in rodents showed anatomical connectivity of RLi with the striatum (strongly with the pallidum), hypothalamus, thalamus, prefrontal cortex, DR, and amygdala (Del-Fava et al., 2007), although its projections did not reach the nucleus accumbens. Our results showed connectivity of the CLi-RLi toward the aforementioned areas, as well as to the basal forebrain label (which includes the accumbens). Further studies might give additional information specifically about the latter connectivity.

The *inferior olivary nucleus (ION)* is implicated in motor learning and motor error correction (e.g., in the coordination and refinement of movements) through its structural connectivity with the cerebellum (Olszewski & Baxter, 2014). This structure is also involved in motor related functions such as learning and timing of movements, as well as in comparing intended versus achieved movements (De Zeeuw et al., 1998); also these functions can be performed due to its close relationship with the cerebellum. Interestingly, in agreement with previous literature, our results showed that ION had anatomical connectivity with the cerebellum, Ve, hypoglossal nucleus (contained in VSM label), SC (involved in the optokinetic reflex response), RN, and cortical motor and somatosensory areas (Barmack, 2006; Stoodley & Schmahmann, 2010). Note that we found strong ipsilateral cortical connectivity, and sparser connectivity in the contralateral brain hemisphere.

The *red nucleus (RN)*, traditionally involved in motor functions and in diseases such as essential tremor (Wills et al., 1994), is still a poorly investigated region of the human brain. In primates, the RN circuitry is anatomically segregated in two connectivity pathways: the rubrospinal pathway and the rubro-olivo-cerebellar one (Basile et al., 2021). We found that both subregions of RN connect to ION, cerebellum, and bilateral frontal cortex, as expected for the rubro-olivo-cerebellar circuit. Previous tractography studies in humans also showed connectivity of the RN toward the pericentral cortex, prefrontal cortex, temporal cortex, striatum and sensorimotor cortex as in the present study (Habas & Cabanis, 2006, 2007). The latter anatomical finding also suggests a possible role of the RN beyond motor tasks, specifically in sensorimotor integration, yet future studies are needed to further investigate this.

4.3 | Translatability to clinical settings

In Figure 12, we show the translatability of the tractography results obtained at 7 Tesla to conventional DWI acquisitions at 3 Tesla. The

association between 7 and 3 Tesla mean connectivity indices was high with a correlation value of 0.57 for all the used targets. The percentage of common links between the two-scanner data decreased with increasing the statistical threshold, showing less percentage of variability for the brainstem targets compared with the total and cortical/subcortical targets (non-brainstem). This might be due to an inherent greater sensitivity of tractography methods to proximal rather than distal brain regions (Morris et al., 2008).

5 | IMPACT

This study provided information about in vivo human structural connectivity of arousal and motor brainstem nuclei based on a recently developed probabilistic brainstem nuclei atlas in living humans. The anatomical connectivity of the studied nuclei showed similarities with previous invasive animal and non-invasive human studies, further validating the probabilistic atlas used and the generated connectome. Using probabilistic tractography of ultra-high field MRI, arousal and motor brainstem nuclei showed connectivity toward specific cortical and subcortical structures, and high brainstem interconnectivity, as expected from the literature (Olszewski & Baxter, 2014; Parvizi, 2001; Satpute et al., 2019). Remarkably important differences were found across nuclei, for example, the presence of connectivity of SubC with the occipital cortex, absent in other nuclei, possibly underlying the generation of ponto-geniculo-occipital waves during REM sleep. We found high interconnectivity within arousal nuclei and with thalamus and hypothalamus, in line with previous research (Bianciardi et al., 2021; Snider et al., 2019), possibly underlying the widespread cortical connectivity of arousal nuclei through multiple pathways. Interestingly, we found similar structural connectivity patterns for locomotor nuclei, that is, CnF, PTg and isRt, suggesting that these brainstem structures interact with each other and are involved in motor behavior. Furthermore, our results showed good translatability of our 7 Tesla findings to 3 Tesla data, with higher association and percentage of common links for brainstem-to-brainstem connectivity. The findings of the present work might serve as a basis for future studies on impaired connectivity in neurological and psychiatric diseases (i.e., disorders of consciousness, sleep disorders, neurodegenerative diseases, depression, anxiety).

6 | LIMITATIONS

Despite recent advances in fiber tracking models, current tractography methods still face limitations in areas of fiber crossing, kissing, or fanning; the brainstem is a funneling area rich of larger and smaller fiber bundles, which might represent a challenge for tractography due to this limitation. We must also keep in mind that tractography is neither able to distinguish the directionality of neuronal transmission nor to disentangle multisynaptic circuits, thereby hindering the interpretation of the flow of information. Future studies might focus on the implementation of recent tractography algorithms

(i.e., anatomically constrained tractography, spherical-deconvolution filtering of tractograms) to possibly obtain higher tracking accuracy of white matter bundles within the brainstem. Nevertheless, these methods rely on a precise definition of the gray matter and white matter masks, which in the brainstem are currently not available. The current study shows the presence within the corpus callosum of streamlines propagated from brainstem nuclei, result not obvious from previous animal literature (Olszewski & Baxter, 2014). This could be ascribed to the polysynaptic nature of tractography reconstructions or to their inability to resolve crossing fibers. Note that, part of the obtained contralateral connectivity stems from fibers decussating in the brainstem, and part from fibers crossing at the level of the corpus callosum. Future work could use regions of interest as constraints for filtering the tractography, and increase the specificity of the connectivity based on animal and ex vivo human literature. Nevertheless, for some nuclei (such as isRt) there is a paucity of information about their connectivity, and for other nuclei, such as LC and other arousal nuclei, the widespread extent of their cortical and subcortical connectivity makes it difficult to properly constrain tractography results. In summary, tractography reconstructions are an indirect measure of the underlying anatomic connectivity.

Our connectome included “macro-regions” derived from FreeSurfer parcellations, yet future studies might further parcellate these regions in subregions (e.g., cerebellar and thalamic subregions) to better understand their anatomical relationships and infer their possible role in more detail in arousal and motor functions.

The brainstem is prone to image distortion (Tang et al., 2018). We performed careful spatial distortion correction using images acquired in two opposite phase encoding directions and cutting-edge correction methods. Nevertheless, residual spatial distortions occurred in some subjects mainly in the anterior part of the pons yet they were not visible in the posterior portion of the brainstem, where the nuclei used in this study were located.

A custom-built 64-channel head coil was used at 3 Tesla. Commercial receiver coils are typically limited to 32 channels for 3 Tesla MRI. Nevertheless, previous work (Keil et al., 2013) shows that the sensitivity of this custom 64-channel coil does not vary significantly in the brainstem compared with that of a commercial 32-channel coil. This suggests the generalizability of our brainstem-to-brainstem results to more widely used 32-channel receiver coils. Conversely, the non-negligible coil sensitivity increase in the cortex (~30%) provided by this 64-channel coil (Keil et al., 2013) might have affected the brainstem-to-cortical connectivity results.

Despite these methodological limitations we provide a wide-ranging human in vivo 2D connectome of arousal and motor brainstem nuclei, which adds to the existing animal literature and is a starting point for future research studies.

7 | CONCLUSIONS

In this study, we provided a structural connectome of arousal and motor brainstem nuclei in living humans, describing their connectivity

to other (e.g., autonomic, sensory) brainstem nuclei, cerebellum, subcortical, and cortical structures. To date, the in vivo mapping of brainstem nuclei has been defiant because the brainstem is a highly complex anatomical area where numerous tiny structures can be found. Yet, these nuclei are not easy to be visualized in conventional imaging. To overcome this limitation, we used an in vivo human probabilistic structural atlas, and performed probabilistic tractography using DWI images acquired at 7 Tesla and at 3 Tesla. After ad-hoc preprocessing, we used cutting-edge coregistration methods and conducted a careful quality control of the anatomical alignment. Finally, by using probabilistic tractography based on constrained spherical deconvolution we built the 2D connectomes of brainstem nuclei that are relevant in arousal and motor functions. Our results showed strong interconnectivity within the arousal and motor brainstem nuclei, and good translatability to conventional (e.g., 3 T) settings. This study might serve as a reference for future anatomical connectivity research of subcortical connectivity in health, and might also provide a baseline for future research of disorders of consciousness, sleep disorders, motor, psychiatric, and neurodegenerative diseases.

ACKNOWLEDGMENTS

MGH-Claffin-Distinguished-Scholar; Harvard-Mind-Brain-Behavior-Faculty-Award; NIH-NIBIB-K01EB019474; NIH-NIDCD-R21DC015888; NIA-R01AG063982. Dr. Thorsten Feiweier for providing the diffusion sequence used in this study.

CONFLICT OF INTEREST

The authors declare no conflicts of interest.

DATA AVAILABILITY STATEMENT

Connectivity data will be shared by request from any qualified investigator.

ETHICS STATEMENT

The study was conducted according to the guidelines of the declaration of Helsinki and approved by the Massachusetts General Hospital Institutional Review Board. All participants gave written informed consent prior to participation.

ORCID

María Guadalupe García-Gomar  <https://orcid.org/0000-0001-5633-3419>

REFERENCES

- Adamantidis, A. R., Gutierrez Herrera, C., & Gent, T. C. (2019). Oscillating circuitries in the sleeping brain. *Nature Reviews Neuroscience*, 20(12), 746–762. <https://doi.org/10.1038/s41583-019-0223-4>
- Avants, B. B., Tustison, N. J., Song, G., Cook, P. A., Klein, A., & Gee, J. C. (2011). A reproducible evaluation of ANTs similarity metric performance in brain image registration. *NeuroImage*, 54(3), 2033–2044. <https://doi.org/10.1016/j.neuroimage.2010.09.025>
- Balázsfi, D. G., Zelena, D., Farkas, L., Demeter, K., Barna, I., Cserép, C., Takács, V. T., Nyíri, G., Göllöncsér, F., Sperlág, B., Freund, T. F., & Haller, J. (2017). Median raphe region stimulation alone generates

- remote, but not recent fear memory traces. *PLoS One*, 12(7), e0181264. <https://doi.org/10.1371/journal.pone.0181264>
- Bari, B., Chokshi, V., & Schmidt, K. (2020). Locus coeruleus-norepinephrine: Basic functions and insights into Parkinson's disease. *Neural Regeneration Research*, 15(6), 1006–1013. <https://doi.org/10.4103/1673-5374.270297>
- Barmack, N. H. (2006). Inferior olive and oculomotor system. In S. Waxman, D. G. Stein, D. Swaab, & H. Fields (Eds.), *Progress in brain research* (Vol. 151, pp. 269–291). Elsevier.
- Barnden, L. R., Shan, Z. Y., Staines, D. R., Marshall-Gradisnik, S., Finegan, K., Ireland, T., & Bhuta, S. (2019). Intra brainstem connectivity is impaired in chronic fatigue syndrome. *NeuroImage: Clinical*, 24, 102045. <https://doi.org/10.1016/j.nicl.2019.102045>
- Basile, G. A., Quartu, M., Bertino, S., Serra, M. P., Boi, M., Bramanti, A., Anastasi, G. P., Milardi, D., & Cacciola, A. (2021). Red nucleus structure and function: From anatomy to clinical neurosciences. *Brain Structure & Function*, 226(1), 69–91. <https://doi.org/10.1007/s00429-020-02171-x>
- Beitz, A. J. (1982). The nuclei of origin of brain stem enkephalin and substance P projections to the rodent nucleus raphe magnus. *Neuroscience*, 7(11), 2753–2768. [https://doi.org/10.1016/0306-4522\(82\)90098-7](https://doi.org/10.1016/0306-4522(82)90098-7)
- Benarroch, E. E. (2012). Periaqueductal gray: An interface for behavioral control. *Neurology*, 78(3), 210–217. <https://doi.org/10.1212/WNL.0b013e31823fcdde>
- Berridge, C. W., & Waterhouse, B. D. (2003). The locus coeruleus-noradrenergic system: Modulation of behavioral state and state-dependent cognitive processes. *Brain Research Reviews*, 42(1), 33–84. [https://doi.org/10.1016/S0165-0173\(03\)00143-7](https://doi.org/10.1016/S0165-0173(03)00143-7)
- Bianciardi, M., Izzy, S., Rosen, B. R., Wald, L. L., & Edlow, B. L. (2021). Location of subcortical microbleeds and recovery of consciousness after severe traumatic brain injury. *Neurology*, 97(2), e113–e123. <https://doi.org/10.1212/WNL.00000000000012192>
- Bianciardi, M., Strong, C., Toschi, N., Edlow, B. L., Fischl, B., Brown, E. N., Rosen, B. R., & Wald, L. L. (2018). A probabilistic template of human mesopontine tegmental nuclei from in vivo 7T MRI. *NeuroImage*, 170, 222–230. <https://doi.org/10.1016/j.neuroimage.2017.04.070>
- Bianciardi, M., Toschi, N., Edlow, B. L., Eichner, C., Setsompop, K., Polimeni, J. R., Brown, E. N., Kinney, H. C., Rosen, B. R., & Wald, L. L. (2015). Toward an in vivo neuroimaging template of human brainstem nuclei of the ascending arousal, autonomic, and motor systems. *Brain Connectivity*, 5(10), 597–607. <https://doi.org/10.1089/brain.2015.0347>
- Bianciardi, M., Toschi, N., Eichner, C., Polimeni, J. R., Setsompop, K., Brown, E. N., Hämäläinen, M. S., Rosen, B. R., & Wald, L. L. (2016). In vivo functional connectome of human brainstem nuclei of the ascending arousal, autonomic, and motor systems by high spatial resolution 7-Tesla fMRI. *Magma*, 29(3), 451–462. <https://doi.org/10.1007/s10334-016-0546-3>
- Boeve, B. F., Silber, M. H., Saper, C. B., Ferman, T. J., Dickson, D. W., Parisi, J. E., Benarroch, E. E., Ahlsgog, J. E., Smith, G. E., Caselli, R. C., Tippman-Peikert, M., Olson, E. J., Lin, S.-C., Young, T., Wszolek, Z., Schenck, C. H., Mahowald, M. W., Castillo, P. R., Del Tredici, K., & Braak, H. (2007). Pathophysiology of REM sleep behaviour disorder and relevance to neurodegenerative disease. *Brain: A Journal of Neurology*, 130(Pt 11), 2770–2788. <https://doi.org/10.1093/brain/awm056>
- Borghammer, P. (2021). The α -synuclein origin and connectome model (SOC model) of Parkinson's disease: Explaining motor asymmetry, non-motor phenotypes, and cognitive decline. *Journal of Parkinson's Disease*, 11(2), 455–474. <https://doi.org/10.3233/JPD-202481>
- Bueno, D., Lima, L. B., Souza, R., Gonçalves, L., Leite, F., Souza, S., Furigo, I. C., Donato, J., & Metzger, M. (2019). Connections of the laterodorsal tegmental nucleus with the habenular-interpeduncular-raphé system. *Journal of Comparative Neurology*, 527(18), 3046–3072. <https://doi.org/10.1002/cne.24729>
- Cacciola, A., Bertino, S., Basile, G. A., Di Mauro, D., Calamuneri, A., Chillemi, G., Duca, A., Bruschetta, D., Flace, P., Favaloro, A., Calabrò, R. S., Anastasi, G., & Milardi, D. (2019). Mapping the structural connectivity between the periaqueductal gray and the cerebellum in humans. *Brain Structure and Function*, 224(6), 2153–2165. <https://doi.org/10.1007/s00429-019-01893-x>
- Cacciola, A., Milardi, D., Basile, G. A., Bertino, S., Calamuneri, A., Chillemi, G., Paladina, G., Impellizzeri, F., Trimarchi, F., Anastasi, G., Bramanti, A., & Rizzo, G. (2019). The cortico-rubral and cerebellorubral pathways are topographically organized within the human red nucleus. *Scientific Reports*, 9(1), 12117. <https://doi.org/10.1038/s41598-019-48164-7>
- Caggiano, V., Leiras, R., Goñi-Erro, H., Masini, D., Bellardita, C., Bouvier, J., Caldeira, V., Fisone, G., & Kiehn, O. (2018). Midbrain circuits that set locomotor speed and gait selection. *Nature*, 553(7689), 455–460. <https://doi.org/10.1038/nature25448>
- Cameron, A. A., Khan, I. A., Westlund, K. N., Cliffer, K. D., & Willis, W. D. (1995). The efferent projections of the periaqueductal gray in the rat: A Phaseolus vulgaris-leucoagglutinin study. I. Ascending projections. *The Journal of Comparative Neurology*, 351(4), 568–584. <https://doi.org/10.1002/cne.903510407>
- Cameron, A. A., Khan, I. A., Westlund, K. N., & Willis, W. D. (1995). The efferent projections of the periaqueductal gray in the rat: A Phaseolus vulgaris-leucoagglutinin study. II. Descending projections. *The Journal of Comparative Neurology*, 351(4), 585–601. <https://doi.org/10.1002/cne.903510408>
- Chang, S. J., Cajigas, I., Opris, I., Guest, J. D., & Noga, B. R. (2020). Dissecting brainstem locomotor circuits: Converging evidence for cuneiform nucleus stimulation. *Frontiers in Systems Neuroscience*, 14, 64. <https://doi.org/10.3389/fnsys.2020.00064>
- Charara, A., & Parent, A. (1998). Chemoarchitecture of the primate dorsal raphe nucleus. *Journal of Chemical Neuroanatomy*, 15(2), 111–127. [https://doi.org/10.1016/S0891-0618\(98\)00036-2](https://doi.org/10.1016/S0891-0618(98)00036-2)
- Coimbra, B., Soares-Cunha, C., Vasconcelos, N. A. P., Domingues, A. V., Borges, S., Sousa, N., & Rodrigues, A. J. (2019). Role of laterodorsal tegmentum projections to nucleus accumbens in reward-related behaviors. *Nature Communications*, 10(1), 4138. <https://doi.org/10.1038/s41467-019-11557-3>
- Cornwall, J., Cooper, J. D., & Phillipson, O. T. (1990). Afferent and efferent connections of the laterodorsal tegmental nucleus in the rat. *Brain Research Bulletin*, 25(2), 271–284. [https://doi.org/10.1016/0361-9230\(90\)90072-8](https://doi.org/10.1016/0361-9230(90)90072-8)
- De Zeeuw, C. I., Simpson, J. I., Hoogenraad, C. C., Galjart, N., Koekkoek, S. K., & Ruigrok, T. J. (1998). Microcircuitry and function of the inferior olive. *Trends in Neurosciences*, 21(9), 391–400. [https://doi.org/10.1016/s0166-2236\(98\)01310-1](https://doi.org/10.1016/s0166-2236(98)01310-1)
- Delano-Wood, L., Bangen, K. J., Sorg, S. F., Clark, A. L., Schiehser, D. M., Luc, N., Bondi, M. W., Werhane, M., Kim, R. T., & Bigler, E. D. (2015). Brainstem white matter integrity is related to loss of consciousness and postconcussive symptomatology in veterans with chronic mild to moderate traumatic brain injury. *Brain Imaging and Behavior*, 9(3), 500–512. <https://doi.org/10.1007/s11682-015-9432-2>
- Del-Fava, F., Hasue, R. H., Ferreira, J. G. P., & Shammah-Lagnado, S. J. (2007). Efferent connections of the rostral linear nucleus of the ventral tegmental area in the rat. *Neuroscience*, 145(3), 1059–1076. <https://doi.org/10.1016/j.neuroscience.2006.12.039>
- Destrieux, C., Fischl, B., Dale, A., & Halgren, E. (2010). Automatic parcellation of human cortical gyri and sulci using standard anatomical nomenclature. *NeuroImage*, 53(1), 1–15. <https://doi.org/10.1016/j.neuroimage.2010.06.010>
- Edlow, B. L., Takahashi, E., Wu, O., Benner, T., Dai, G., Bu, L., Grant, P. E., Greer, D. M., Greenberg, S. M., Kinney, H. C., & Folkerth, R. D. (2012). Neuroanatomic connectivity of the human ascending arousal system critical to consciousness and its disorders. *Journal of Neuropathology & Experimental Neurology*, 71(6), 531–546. <https://doi.org/10.1097/NEN.0b013e3182588293>

- Englot, D. J., Gonzalez, H. F. J., Reynolds, B. B., Konrad, P. E., Jacobs, M. L., Gore, J. C., Landman, B. A., & Morgan, V. L. (2018). Relating structural and functional brainstem connectivity to disease measures in epilepsy. *Neurology*, 91(1), e67–e77. <https://doi.org/10.1212/WNL.0000000000005733>
- Ferreira, A. N., Yousuf, H., Dalton, S., & Sheets, P. L. (2015). Highly differentiated cellular and circuit properties of infralimbic pyramidal neurons projecting to the periaqueductal gray and amygdala. *Frontiers in Cellular Neuroscience*, 9, 161. <https://doi.org/10.3389/fncel.2015.00161>
- Flores, J. A., Galan-Rodríguez, B., Ramiro-Fuentes, S., & Fernandez-Espejo, E. (2006). Role for dopamine neurons of the rostral linear nucleus and periaqueductal gray in the rewarding and sensitizing properties of heroin. *Neuropsychopharmacology*, 31(7), 1475–1488. <https://doi.org/10.1038/sj.npp.1300946>
- French, I. T., & Muthusamy, K. A. (2018). A review of the pedunculopontine nucleus in Parkinson's disease. *Frontiers in Aging Neuroscience*, 10, 99. <https://doi.org/10.3389/fnagi.2018.00099>
- García-Gomar, M. G., Strong, C., Toschi, N., Singh, K., Rosen, B. R., Wald, L. L., & Bianciardi, M. (2019). In vivo probabilistic structural atlas of the inferior and superior colliculi, medial and lateral geniculate nuclei and superior olivary complex in humans based on 7 Tesla MRI. *Frontiers in Neuroscience*, 13, 764. <https://doi.org/10.3389/fnins.2019.00764>
- García-Gomar, M. G., Videnovic, A., Singh, K., Stauder, M., Lewis, L. D., Wald, L. L., Rosen, B. R., & Bianciardi, M. (2021). Disruption of brainstem structural connectivity in REM sleep behavior disorder using 7 Tesla magnetic resonance imaging. *Movement Disorders*, mds.28895, 847–853. <https://doi.org/10.1002/mds.28895>
- García-Lorenzo, D., Longo-Dos Santos, C., Ewencyk, C., Leu-Semenescu, S., Gallea, C., Quattrocchi, G., Pita Lobo, P., Poupon, C., Benali, H., Arnulf, I., Vidailhet, M., & Lehericy, S. (2013). The coeruleus/subcoeruleus complex in rapid eye movement sleep behaviour disorders in Parkinson's disease. *Brain*, 136(7), 2120–2129. <https://doi.org/10.1093/brain/awt152>
- García-Rill, E., Saper, C. B., Rye, D. B., Kofler, M., Nonnekes, J., Lozano, A., Valls-Solé, J., & Hallett, M. (2019). Focus on the pedunculopontine nucleus. Consensus review from the May 2018 brainstem society meeting in Washington, DC, USA. *Clinical Neurophysiology*, 130(6), 925–940. <https://doi.org/10.1016/j.clinph.2019.03.008>
- Graf, W. M., & Ugolini, G. (2006). The central mesencephalic reticular formation: Its role in space-time coordinated saccadic eye movements: Perspectives. *The Journal of Physiology*, 570(3), 433–434. <https://doi.org/10.1113/jphysiol.2005.103184>
- Guyenet, P. G., & Abbott, S. B. G. (2013). Chemoreception and asphyxia-induced arousal. *Respiratory Physiology & Neurobiology*, 188(3), 333–343. <https://doi.org/10.1016/j.resp.2013.04.011>
- Habas, C., & Cabanis, E. A. (2006). Cortical projections to the human red nucleus: A diffusion tensor tractography study with a 1.5-T MRI machine. *Neuroradiology*, 48(10), 755–762. <https://doi.org/10.1007/s00234-006-0117-9>
- Habas, C., & Cabanis, E. A. (2007). Cortical projection to the human red nucleus: Complementary results with probabilistic tractography at 3 T. *Neuroradiology*, 49(9), 777–784. <https://doi.org/10.1007/s00234-007-0260-y>
- Holstege, G. (1988). Brainstem-spinal cord projections in the cat, related to control of head and axial movements. *Reviews of Oculomotor Research*, 2, 431–470.
- Hornung, J.-P. (2003). The human raphe nuclei and the serotonergic system. *Journal of Chemical Neuroanatomy*, 26(4), 331–343. <https://doi.org/10.1016/j.jchemneu.2003.10.002>
- Huang, K. W., Ochandarena, N. E., Philson, A. C., Hyun, M., Birnbaum, J. E., Cicconet, M., & Sabatini, B. L. (2019). Molecular and anatomical organization of the dorsal raphe nucleus. *eLife*, 8, e46464. <https://doi.org/10.7554/eLife.46464>
- Huerta, M. F., & Kaas, J. H. (1990). Supplementary eye field as defined by intracortical microstimulation: Connections in macaques. *The Journal of Comparative Neurology*, 293(2), 299–330. <https://doi.org/10.1002/cne.902930211>
- Huerta, M. F., Krubitzer, L. A., & Kaas, J. H. (1986). Frontal eye field as defined by intracortical microstimulation in squirrel monkeys, owl monkeys, and macaque monkeys: I. subcortical connections. *The Journal of Comparative Neurology*, 253(4), 415–439. <https://doi.org/10.1002/cne.902530402>
- Irimia, A., Chambers, M. C., Torgerson, C. M., & Van Horn, J. D. (2012). Circular representation of human cortical networks for subject and population-level connectomic visualization. *NeuroImage*, 60(2), 1340–1351. <https://doi.org/10.1016/j.neuroimage.2012.01.107>
- Keil, B., Blau, J. N., Biber, S., Hoecht, P., Tountcheva, V., Setsompop, K., Triantafyllou, C., & Wald, L. L. (2013). A 64-channel 3T array coil for accelerated brain MRI. *Magnetic Resonance in Medicine*, 70(1), 248–258. <https://doi.org/10.1002/mrm.24427>
- Keil, B., Triantafyllou, C., Hamm, M., & Wald, L. L. (2010). Design optimization of a 32-channel head coil at 7 T. In: Proceedings of the annual meeting of the international society for magnetic resonance in medicine, Stockholm. 1493.
- Kuyper, H. G. J. M., & Lawrence, D. G. (1967). Cortical projections to the red nucleus and the brain stem in the rhesus monkey. *Brain Research*, 4(2–3), 151–188. [https://doi.org/10.1016/0006-8993\(67\)90004-2](https://doi.org/10.1016/0006-8993(67)90004-2)
- Lee, H. J. (2006). Role of substantia nigra-amygdala connections in surprise-induced enhancement of attention. *Journal of Neuroscience*, 26(22), 6077–6081. <https://doi.org/10.1523/JNEUROSCI.1316-06.2006>
- Liu, S., Aungst, J. L., Puche, A. C., & Shipley, M. T. (2012). Serotonin modulates the population activity profile of olfactory bulb external tufted cells. *Journal of Neurophysiology*, 107(1), 473–483. <https://doi.org/10.1152/jn.00741.2011>
- Lu, J. (2006). Identification of wake-active dopaminergic neurons in the ventral periaqueductal gray matter. *Journal of Neuroscience*, 26(1), 193–202. <https://doi.org/10.1523/JNEUROSCI.2244-05.2006>
- Manjón, J. V., Coupé, P., Concha, L., Buades, A., Collins, D. L., & Robles, M. (2013). Diffusion weighted image denoising using overcomplete local PCA. *PLoS One*, 8(9), e73021. <https://doi.org/10.1371/journal.pone.0073021>
- Manto, M., Bower, J. M., Conforto, A. B., Delgado-García, J. M., da Guarda, S. N. F., Gerwig, M., Habas, C., Hagura, N., Ivry, R. B., Mariën, P., Molinari, M., Naito, E., Nowak, D. A., Taib, O. B., Pelisson, D., Tesche, C. D., Tilikete, C., & Timmann, D. (2012). Consensus paper: Roles of the cerebellum in motor control—The diversity of ideas on cerebellar involvement in movement. *The Cerebellum*, 11(2), 457–487. <https://doi.org/10.1007/s12311-011-0331-9>
- Matsumura, M., Nambu, A., Yamaji, Y., Watanabe, K., Imai, H., Inase, M., Tokuno, H., & Takada, M. (2000). Organization of somatic motor inputs from the frontal lobe to the pedunculopontine tegmental nucleus in the macaque monkey. *Neuroscience*, 98(1), 97–110. [https://doi.org/10.1016/S0306-4522\(00\)00099-3](https://doi.org/10.1016/S0306-4522(00)00099-3)
- Mena-Segovia, J., Bolam, J. P., & Magill, P. J. (2004). Pedunculopontine nucleus and basal ganglia: Distant relatives or part of the same family? *Trends in Neurosciences*, 27(10), 585–588. <https://doi.org/10.1016/j.tins.2004.07.009>
- Merel, J., Botvinick, M., & Wayne, G. (2019). Hierarchical motor control in mammals and machines. *Nature Communications*, 10(1), 5489. <https://doi.org/10.1038/s41467-019-13239-6>
- Mesulam, M.-M., Geula, C., Bothwell, M. A., & Hersh, L. B. (1989). Human reticular formation: Cholinergic neurons of the pedunculopontine and laterodorsal tegmental nuclei and some cytochemical comparisons to forebrain cholinergic neurons. *The Journal of Comparative Neurology*, 283(4), 611–633. <https://doi.org/10.1002/cne.902830414>
- Molliver, M. E. (1987). Serotonergic neuronal systems: What their anatomical organization tells us about function. *Journal of Clinical Psychopharmacology*, 7(6 Suppl), 3S–23S.
- Morris, D. M., Embleton, K. V., & Parker, G. J. M. (2008). Probabilistic fibre tracking: Differentiation of connections from chance events.

- NeuroImage*, 42(4), 1329–1339. <https://doi.org/10.1016/j.neuroimage.2008.06.012>
- Moruzzi, G., & Magoun, H. W. (1949). Brain stem reticular formation and activation of the EEG. *Electroencephalography and Clinical Neurophysiology*, 11(4), 455–473. [https://doi.org/10.1016/0013-4694\(49\)90219-9](https://doi.org/10.1016/0013-4694(49)90219-9)
- Muthusamy, K. A., Aravamuthan, B. R., Kringelbach, M. L., Jenkinson, N., Voets, N. L., Johansen-Berg, H., Stein, J. F., & Aziz, T. Z. (2007). Connectivity of the human pedunculo-pontine nucleus region and diffusion tensor imaging in surgical targeting. *Journal of Neurosurgery*, 107(4), 814–820. <https://doi.org/10.3171/JNS-07/10/0814>
- Olszewski, J., & Baxter, D. (2014). *Cytoarchitecture of the human brain stem* (3rd ed.). Karger.
- Pahapill, P. A. (2000). The pedunculo-pontine nucleus and Parkinson's disease. *Brain*, 123(9), 1767–1783. <https://doi.org/10.1093/brain/123.9.1767>
- Parent, A., Mackey, A., Smith, Y., & Boucher, R. (1983). The output organization of the substantia nigra in primate as revealed by a retrograde double labeling method. *Brain Research Bulletin*, 10(4), 529–537. [https://doi.org/10.1016/0361-9230\(83\)90151-X](https://doi.org/10.1016/0361-9230(83)90151-X)
- Parvizi, J., & Damasio, A. (2001). Consciousness and the brainstem. *Cognition*, 79, 135–160. [https://doi.org/10.1016/s0010-0277\(00\)00127-x](https://doi.org/10.1016/s0010-0277(00)00127-x)
- Pauli, W. M., Nili, A. N., & Tyszka, J. M. (2018). A high-resolution probabilistic in vivo atlas of human subcortical brain nuclei. *Scientific Data*, 5, 180063. <https://doi.org/10.1038/sdata.2018.63>
- Paxinos, G., & Mai, J. K. (2007). *The human nervous system*. Elsevier B.V.
- Paxinos, G., Xu-Feng, H., Sengul, G., & Watson, C. (2012). Organization of brainstem nuclei. In *The human nervous system*. Elsevier.
- Redgrave, P., Vautrelle, N., & Reynolds, J. N. J. (2011). Functional properties of the basal ganglia's re-entrant loop architecture: Selection and reinforcement. *Neuroscience*, 198, 138–151. <https://doi.org/10.1016/j.neuroscience.2011.07.060>
- Robinson, F. R., Phillips, J. O., & Fuchs, A. F. (1994). Coordination of gaze shifts in primates: Brainstem inputs to neck and extraocular motoneuron pools. *The Journal of Comparative Neurology*, 346(1), 43–62. <https://doi.org/10.1002/cne.903460104>
- Rodrigo-Angulo, M. L., Rodríguez-Veiga, E., & Reinoso-Suárez, F. (2000). Serotonergic connections to the ventral oral pontine reticular nucleus: Implication in paradoxical sleep modulation. *The Journal of Comparative Neurology*, 418(1), 93–105. [https://doi.org/10.1002/\(sici\)1096-9861\(20000228\)418:1<93::aid-cne7>3.0.co;2-1](https://doi.org/10.1002/(sici)1096-9861(20000228)418:1<93::aid-cne7>3.0.co;2-1)
- Rodrigo-Angulo, M. L., Rodríguez-Veiga, E., & Reinoso-Suárez, F. (2005). A quantitative study of the brainstem cholinergic projections to the ventral part of the oral pontine reticular nucleus (REM sleep induction site) in the cat. *Experimental Brain Research*, 160(3), 334–343. <https://doi.org/10.1007/s00221-004-2015-x>
- Rubinov, M., & Sporns, O. (2010). Complex network measures of brain connectivity: Uses and interpretations. *NeuroImage*, 52(3), 1059–1069. <https://doi.org/10.1016/j.neuroimage.2009.10.003>
- Saper, C. B., Chou, T. C., & Scammell, T. E. (2001). The sleep switch: Hypothalamic control of sleep and wakefulness. *Trends in Neurosciences*, 24(12), 726–731. [https://doi.org/10.1016/S0166-2236\(00\)02002-6](https://doi.org/10.1016/S0166-2236(00)02002-6)
- Saper, C. B., Fuller, P. M., Pedersen, N. P., Lu, J., & Scammell, T. E. (2010). Sleep state switching. *Neuron*, 68(6), 1023–1042. <https://doi.org/10.1016/j.neuron.2010.11.032>
- Satpute, A. B., Kragel, P. A., Barrett, L. F., Wager, T. D., & Bianciardi, M. (2019). Deconstructing arousal into wakeful, autonomic and affective varieties. *Neuroscience Letters*, 693, 19–28. <https://doi.org/10.1016/j.neulet.2018.01.042>
- Séguéla, P., Watkins, K. C., Geffard, M., & Descarries, L. (1990). Noradrenaline axon terminals in adult rat neocortex: An immunocytochemical analysis in serial thin sections. *Neuroscience*, 35(2), 249–264. [https://doi.org/10.1016/0306-4522\(90\)90079-J](https://doi.org/10.1016/0306-4522(90)90079-J)
- Sharma, Y., Xu, T., Graf, W. M., Fobbs, A., Sherwood, C. C., Hof, P. R., Allman, J. M., & Manaye, K. F. (2010). Comparative anatomy of the locus coeruleus in humans and nonhuman primates. *The Journal of Comparative Neurology*, 518(7), 963–971. <https://doi.org/10.1002/cne.22249>
- Shik, M. L., Severin, F. V., & Orlovskii, G. N. (1966). Control of walking and running by means of electric stimulation of the midbrain. *Biofizika*, 11(4), 659–666.
- Simon, C., Hayar, A., & Garcia-Rill, E. (2012). Developmental changes in glutamatergic fast synaptic neurotransmission in the dorsal sub-coeruleus nucleus. *Sleep*, 35(3), 407–417. <https://doi.org/10.5665/sleep.1706>
- Singh, K., García-Gomar, M. G., & Bianciardi, M. (2021). Probabilistic atlas of the mesencephalic reticular formation, isthmus reticular formation, microcellular tegmental nucleus, ventral tegmental area nucleus complex, and caudal–rostral linear raphe nucleus complex in living humans from 7 Tesla magnetic resonance imaging. *Brain Connectivity*, 11, 613–623. <https://doi.org/10.1089/brain.2020.0975>
- Singh, K., Indovina, I., Augustinack, J. C., Nestor, K., García-Gomar, M. G., Staab, J. P., & Bianciardi, M. (2020). Probabilistic template of the lateral parabrachial nucleus, medial parabrachial nucleus, vestibular nuclei complex, and medullary viscerosensory-motor nuclei complex in living humans from 7 Tesla MRI. *Frontiers in Neuroscience*, 13, 1425. <https://doi.org/10.3389/fnins.2019.01425>
- Snider, S. B., Bodien, Y. G., Bianciardi, M., Brown, E. N., Wu, O., & Edlow, B. L. (2019). Disruption of the ascending arousal network in acute traumatic disorders of consciousness. *Neurology*, 93(13), e1281–e1287. <https://doi.org/10.1212/WNL.00000000000008163>
- Stefani, A., Peppe, A., Galati, S., Bassi, M. S., D'Angelo, V., & Pierantozzi, M. (2013). The serendipity case of the pedunculo-pontine nucleus low-frequency brain stimulation: Chasing a gait response, finding sleep, and cognition improvement. *Frontiers in Neurology*, 4, 68. <https://doi.org/10.3389/fneur.2013.00068>
- Stoodley, C. J., & Schmahmann, J. D. (2010). Evidence for topographic organization in the cerebellum of motor control versus cognitive and affective processing. *Cortex*, 46(7), 831–844. <https://doi.org/10.1016/j.cortex.2009.11.008>
- Takakusaki, K., Habaguchi, T., Ohtinata-Sugimoto, J., Saitoh, K., & Sakamoto, T. (2003). Basal ganglia efferents to the brainstem centers controlling postural muscle tone and locomotion: A new concept for understanding motor disorders in basal ganglia dysfunction. *Neuroscience*, 119(1), 293–308. [https://doi.org/10.1016/S0306-4522\(03\)00095-2](https://doi.org/10.1016/S0306-4522(03)00095-2)
- Tang, Y., Sun, W., Toga, A. W., Ringman, J. M., & Shi, Y. (2018). A probabilistic atlas of human brainstem pathways based on connectome imaging data. *NeuroImage*, 169, 227–239. <https://doi.org/10.1016/j.neuroimage.2017.12.042>
- Tournier, J.-D., Calamante, F., & Connelly, A. (2007). Robust determination of the fibre orientation distribution in diffusion MRI: Non-negativity constrained super-resolved spherical deconvolution. *NeuroImage*, 35(4), 1459–1472. <https://doi.org/10.1016/j.neuroimage.2007.02.016>
- Tournier, J.-D., Calamante, F., & Connelly, A. (2010). Improved probabilistic streamlines tractography by 2nd order integration over fibre orientation distributions. *Proceedings of the International Society for Magnetic Resonance in Medicine*, 1670.
- Valencia Garcia, S., Brischoux, F., Clément, O., Libourel, P.-A., Arthaud, S., Lazarus, M., Luppi, P.-H., & Fort, P. (2018). Ventromedial medulla inhibitory neuron inactivation induces REM sleep without atonia and REM sleep behavior disorder. *Nature Communications*, 9(1), 504. <https://doi.org/10.1038/s41467-017-02761-0>
- Varentsova, A., Zhang, S., & Arfanakis, K. (2014). Development of a high angular resolution diffusion imaging human brain template. *NeuroImage*, 91, 177–186. <https://doi.org/10.1016/j.neuroimage.2014.01.009>
- Vertes, R. P. (2010). Serotonergic regulation of rhythmical activity of the brain, concentrating on the hippocampus. In E. C. Azmitia (Ed.),

- Handbook of behavioral neuroscience* (Vol. 21, pp. 277–292). Elsevier. [https://doi.org/10.1016/S1569-7339\(10\)70084-9](https://doi.org/10.1016/S1569-7339(10)70084-9)
- Wang, D. V., Yau, H.-J., Broker, C. J., Tsou, J.-H., Bonci, A., & Ikemoto, S. (2015). Mesopontine median raphe regulates hippocampal ripple oscillation and memory consolidation. *Nature Neuroscience*, 18(5), 728–735. <https://doi.org/10.1038/nn.3998>
- Wang, J., Wang, X., Xia, M., Liao, X., Evans, A., & He, Y. (2015). GREYNA: A graph theoretical network analysis toolbox for imaging connectomics. *Frontiers in Human Neuroscience*, 9, 386. <https://doi.org/10.3389/fnhum.2015.00386>
- Watson, T. C., Cerminara, N. L., Lumb, B. M., & Apps, R. (2016). Neural correlates of fear in the periaqueductal gray. *The Journal of Neuroscience*, 36(50), 12707–12719. <https://doi.org/10.1523/JNEUROSCI.1100-16.2016>
- Wills, A. J., Jenkins, I. H., Thompson, P. D., Findley, L. J., & Brooks, D. J. (1994). Red nuclear and cerebellar but no olivary activation associated with essential tremor: A positron emission tomographic study. *Annals of Neurology*, 36(4), 636–642. <https://doi.org/10.1002/ana.410360413>
- Zhang, Y., Larcher, K. M.-H., Mistic, B., & Dagher, A. (2017). Anatomical and functional organization of the human substantia nigra and its connections. *eLife*, 6, e26653. <https://doi.org/10.7554/eLife.26653>
- Zhang, Y., Vakhtin, A. A., Jennings, J. S., Massaband, P., Wintermark, M., Craig, P. L., Ashford, J. W., Clark, J. D., & Furst, A. J. (2020). Diffusion tensor tractography of brainstem fibers and its application in pain. *PLoS One*, 15(2), e0213952. <https://doi.org/10.1371/journal.pone.0213952>

SUPPORTING INFORMATION

Additional supporting information may be found in the online version of the article at the publisher's website.

How to cite this article: García-Gomar, M. G., Singh, K., Cauzzo, S., & Bianciardi, M. (2022). In vivo structural connectome of arousal and motor brainstem nuclei by 7 Tesla and 3 Tesla MRI. *Human Brain Mapping*, 1–25. <https://doi.org/10.1002/hbm.25962>